INTERNATIONAL ATOMIC ENERGY AGENCY
UNITED NATIONS EDUCATIONAL, SCIENTIFIC AND CULTURAL ORGANIZATION

INTERNATIONAL CENTRE FOR THEORETICAL PHYSICS
34100 TRIESTE (ITALY) - P.O.B. 586 - MIRAMARE - STRADA COSTIERA 11 - TELEPHONES: 224281/2/3/4/5/6
CABLE: CENTRATOM - TELEX 460392-1

SMR/110/A - 11

WORKING PARTY
ON
"PHYSICS OF CONDENSED MATTER AT PLANETARY PRESSURES"
(20 August - 7 September 1984)

MATTER UNDER EXTREME CONDITIONS OF TEMPERATURE AND PRESSURE *

M. ROSS

Lawrence Livermore Laboratory, Univ. of California,
Livermore, California 94550, USA

* UCRL Preprint No. 90856

CONTENTS

Abstract

Research on matter at extreme conditions has provided new insights into material behavior at atmospheric pressure. The application of high pressure is the simplest way to change the lattice spacing and has led to the discovery of new phenomena, new phases, and new forms of electronic and ionic order. The application of high temperatures leads to melting, atomic and electronic excitation, and eventually to ionization and the formation of a plasma state. The combination of high pressures and temperatures continues to present a severe challenge to experimental and theoretical advances. However, current experimental methods permit material studies at pressures of several megabar and temperatures of tens of thousands of degrees Kelvin. The rapid surge in computer technology has in turn permitted the solution of many previously intractable theoretical problems. High-pressure research supplies information about the properties of geologic materials which, when coupled with data from seismic waves and space probes, provides information about the structure of planetary interiors.

1.0 Introduction

The study of matter under extreme conditions is a highly interdisciplinary subject with broad applications to materials science, geophysics, and astrophysics. High-pressure properties are studied in the laboratory using static and dynamic techniques. The two differ drastically in the methods of generating and measuring pressure and in the fundamentally different nature of the final compressed state.

In static experiments the sample is squeezed between a set of opposing pistons or anvils. Temperatures seldom exceed several hundred centigrade. The maximum pressures obtained are currently well below 1 Mbar, limited by the strengths of the available construction materials. Shock compression studies obtain high pressures and temperatures by introducing a rapid impulse into a substance through the detonation of a high explosive, the impact of a high-speed projectile, or the absorption of an intense pulse of radiation. High-speed optical and electronic methods are necessary to measure certain dynamic variables which determine pressure, density and energy. In shock wave experiments, the passage-time of the shock is short compared to the disassembly or "fly away" time of the sample. As a result the attainable pressures for a given material are limited only by the energy density supplied by the driver. Chemical explosives have been used to obtain pressures up to 1 Mbar in liquids and up to 13 Mbar in metals, with accompanying temperatures of tens of thousands of Kelvin. Final pressures ranging from 20 to 158 Mbar have been reported using undergound nuclear explosions. In inertial confinement studies, pellets of liquid deuterium are subjected briefly to laser-driven dynamic pressures of about 1000 Mbar and temperatures in excess of 10^7 K.

The universe is a natural high-pressure laboratory where existing conditions may dwarf any conditions attainable in terrestrial laboratories. The center of the Earth has pressures of about 3.5 Mbar and temperatures of 4000 K. The conditions in Jupiter's center are believed to be about 100 Mbar and 24,000 K. The centers of stars and white dwarfs have pressures in excess of thousands of Mbar and with temperatures of tens of millions of K. In neutron stars pressures of millions of Mbar are believed to exist. In an indirect way physicists have access to a laboratory in which densities go beyond 10^{15} g/cm^3.

This report is organized into four major sections. Section 2 is a review of some of the methods used for obtaining extreme conditions in a controlled environment. These are mainly dynamic methods but, for the sake of completeness, we include a brief description of the diamond anvil cell method now widely used for static studies. In Section 3 we discuss the theory and behavior of condensed matter, and in Section 4 we discuss the subject of fluids and plasmas . Some applications to geophysical problems are reviewed in Section 5.

The subject matter of this report covers a very broad range of conditions, intended to present an overview of important recent developments and to emphasize the behavior of materials and the kinds of properties now being studied. In the present survey these are mainly thermodynamic properties. Applications to conditions which exist in white dwarfs and neutron stars, where strong gravitational fields, radiation pressure, and elementary particles exert a significant influence, are beyond the scope of the present report.

2.0 Experimental Methods

Systematic investigations of high-pressure properties date back to the 18th century (Bridgman, 1958). By the latter part of the 19th Century, Amagat had extended the pressure measurements on gases to about 3 kbar. P. W. Bridgman, of Harvard, ushered in the modern age of high-pressure technology. Bridgman was actively engaged in high-pressure research from 1906 to his death in 1954, and received a Nobel prize in 1946. Near the end of his career he was consistently making measurements above 100 kbar.

During and immediately after World War II, shock-wave research appears to have developed independently in the United States and the U.S.S.R. References to the early history can be found in the reviews by Rice et al. (1958), and Al'tshuler (1965). With few exceptions, the leading practitioners have long been associated with weapons laboratories, primarily in the United States and the U.S.S.R., more recently in France, Japan and several other countries. Compared to static studies, shock-wave research is expensive, requires a much larger support system, and is not likely to become as widespread as static methods without a change in the present technology.

2.1 Diamond Anvil Cell (DAC)

A representative account of current high-pressure research is to be found in the proceedings of the bi-annual AIRAPT Conferences (Homan et al., 1984). The most important recent advance in static high-pressure research has been the development of the diamond anvil cell (DAC) (Jayaraman, 1984, 1983; Bassett, 1979; Block and Piermarini, 1976). A sample may be subjected to nearly megabar pressures when the opposing flat parallel faces of two diamond anvils are pressed together (Fig. 1). The entire pressure-generating cell assembly including DAC can fit into the palm of a hand. The essential feature of this cell comes not only from the hardness of the diamond but also from its transparency to both x-ray and visible light, which permits a variety of measurements on 1- to 20-μm-sized samples. Optical absorption, reflectivity measurements, Raman and Brillouin scattering studies, and x-ray diffraction studies have become possible at extreme pressures. Pressure may be determined by measuring the density of a secondary standard such as NaCl (Bean et al., 1982), or by recording the shift in frequency of the R_1 ruby fluorescence which has been calibrated against shock-wave data (Mao et al., 1978). Recently, Goettel et al. (1984) have reached pressures estimated to be about 2.5 Mbar using ruby alone. They report that above 1.8 Mbar it becomes difficult to measure pressures because the intensity of the R_1 peak decreases significantly. The practical limit for measurement with a sample is imposed by the high probability of fracture near 1 Mbar.

2.2 Shock Compression

A shock wave is a disturbance propagating at supersonic speed in a material, preceded by an extremely rapid rise in pressure, density and temperature. The general reader often associates shock-waves with explosions and other uncontrolled and irreversible processes. Although shock waves are irreversible, the process is well understood and can be controlled to produce a desired response (Rice et al., 1958; Duvall and Fowles, 1963; Al'tshuler, 1965; Zeldovich and Raizer, 1966; Davison and Graham, 1978; Nellis, 1983).

Figure 2 illustrates a one-dimensional, steady, planar shock wave moving at a velocity U_s generated by accelerating a piston from rest to some final constant velocity U_p referred to as the mass- or particle-velocity. The width of the discontinuity is generally a few molecular mean-free-path lengths. The thermodynamic pressure, volume, and energy (P, V, E) behind the

shock front, are related to the initial properties (P_0, V_0, E_0) in front of the shock-wave by the dynamic variables U_s and U_p through the Rankine-Hugoniot equations: conservation of mass,

$$\frac{V}{V_0} = 1 - \frac{U_p}{U_s} \qquad (2.1)$$

conservation of momentum,

$$P - P_0 = U_s U_p / V_0 \qquad (2.2)$$

and conservation of energy

$$E - E_0 = \frac{1}{2} (P + P_0) (V_0 - V) \quad . \qquad (2.3)$$

Thus a measurement of U_s and U_p, with a knowledge of initial conditions, is sufficient to determine the P, V, E of the compressed state. The resulting P-V curve is known as a Hugoniot and represents the locus of points that can be reached from an initial condition. Figure 3 shows some sample Hugoniots for various metals. In the U_s-U_p plane, experimental shock data may be approximated by simple analytical functions

$$U_s = a_0 + a_1 U_p + a_2 U_p^2 + \ldots \qquad (2.4)$$

These are often linear over the entire experimental region, or sometimes the data can be represented using several linear segments. We expect a_0 to correspond to the low-pressure sound speed.

The temperature cannot be obtained from the Rankine-Hugoniot equations, but must be derived from an equation of state. In a few cases it has been determined from a direct measurement of the emitted radiation (Sec. 2.3). The assumptions made in deriving the Hugoniot equations were one-dimensional motion, thermodynamic equilibrium immediately ahead of and behind the shock-front, and negligible material strength. The first assumption can be met experimentally. The second will hold if the electronic and atomic relaxation times are much less than the experimental time scale of about 0.2 μs. The third is justified for pressures appreciably greater than the yield-strength of the material. Typical yield-strengths in metals are 20 kbar

and much less for most materials. Strength effects in shocked solids are reviewed by Davison and Graham (1979).

In the earliest experiments with solids (Rice et al., 1958), high-explosive lens systems (Fig. 4a) consisting of both a fast- and a slow-detonating explosive were used to produce a planar shock-wave which passed through the metal driver plate and into the samples. A series of shorting electrical contact pins placed at various depths in the sample plate served to determine the shock arrival time, hence the shock velocity (U_s). A second series of pins arranged at several free-run distances from the sample surface recorded the free surface velocity (U_{fs}). At present, optical and photographic methods are also widely used (Graham and Asay, 1978). For pressures up to a few hundred kbar $U_p = U_{fs}/2$, and P, V, E may be determined using Eqs. 2.1 -- 2.3. At higher pressures U_p must be evaluated by an iterative procedure using an equation of state calculated from the Hugoniot data. With this method, pressures of several hundred kbar could be obtained.

Subsequent improvements, leading to pressures of several Mbar, were achieved by allowing the rapidly expanding product gases to accelerate the driver plate (Fig. 4b) over a free-run distance before impacting the sample. Currently, the most advanced method for shock loading employs smooth-bore guns driven by compressed gases (Jones et al., 1966; Fowles et al., 1970; Mitchell and Nellis, 1981). One such facility is the Lawrence Livermore National Laboratory (LLNL) two-stage light-gas gun illustrated in Fig. 5. Consider an experiment in which an Al projectile (impactor) is propelled by the gun and strikes a stationary Al target (Fig. 6a). The impactor velocity, U_I, is measured directly by flash x-ray methods. On contact (Fig. 6b), the impactor slows to the velocity U_p, pushing against the target and (as in Fig. 2) acting as a piston driving the shock before it. The shock velocity (U_s) may be determined by placing several pins along the target. For the case of symmetric impact (e.g. Al-Al), U_p is determined from momentum conservation by

$$U_p = \frac{U_I}{2} \quad . \qquad (2.5)$$

Pressures to about 1 Mbar can be achieved in aluminum with this method. The attainable range can be extended by using a stiffer material such as Ta as the impactor (Ta-Al). In this case U_p is not equal to $U_I/2$, but this

difficulty can be overcome if the Hugoniot of Ta has been previously determined by a series of Ta on Ta impact experiments. On the pressure-velocity plane (Fig. 7a), the pressure of the Ta impactor is represented by a curve whose distance from the origin in the velocity coordinate is the free impactor velocity U_I. A measurement of the U_s in the Al target then fixes the slope of the impedance line $P = (\rho_0 U_s) U_p$ (Eq. 2.2). The initial pressure, P_0, is typically negligible. The intersection of the two curves determines the matching conditions of equal P and U_p in Ta and Al and are the conditions reached in Al. In this way the Al data is extended to 1.7 Mbar.

In many circumstances it is necessary to introduce an intermediate baseplate or standard with a known P-U_p between the impactor and sample (Fig. 6c). For example, in experiments with liquids the sample must be placed in a container which necessarily acts as a baseplate. Thus a measurement of U_I, or U_s in the baseplate standard, is sufficient to determine U_p and P in the baseplate. The shock wave subsequently passes into the sample where its velocity is determined by an array of detectors. If the sample has a larger shock impedance ($\rho_0 U_s$) than the baseplate, then a shock wave will also be reflected back. If the sample has a lower impedance, which is typical of liquids, then an expansion wave will pass back into the baseplate, causing the baseplate to unload isentropically. In each case a shock is transmitted to the sample, and the interface matching conditions require that P and U_p be equal. These may be graphically determined in Fig. 7b where the known P-U_p curve for the baseplate (OA) is shown. The determination of U_s in the baseplate standard locates the P-U_p point. A measurement of U_s in the sample is shown as a dashed line. If the sample has a lower impedance, then the intersection of the standard expansion path with line OC determines P and U_p in the sample. If the sample had the larger impedance, the baseplate material shocks up to the line (OB) and the P-U_p point determined by the intersection. This procedure is known as impedance matching and requires a carefully determined standard for a baseplate. To a first approximation the release isentrope or the reflected Hugoniot of the standard may be determined by reflecting line OA. For accurate work it is necessary to calculate these curves with a theoretical equation of state determined from the shock-wave data. By carrying out a series of experiments, all starting from the same initial conditions but employing different projectile velocities, a locus of P, V, E points (Hugoniot) can be reached (Fig. 3).

A considerable variation in the path of the Hugoniot can be achieved by means of double-shock experiments, as shown in the case of liquid deuterium (Fig. 8a). Calculated temperatures include effects of molecular dissociation. Here, the primary shock is passed through the material and then reflected from a high-impedance anvil (Fig. 6d) such as an Al or Cu plate. The reflected wave then compresses the already-compressed material to a higher pressure. By measuring U_s in the anvil-standard, the impedance matching method can be used to determine P-U_p in the reshocked state. At the same density, the temperatures and pressures along the reflected Hugoniot are much lower than those reached by the principal (single shock) Hugoniot, and tend toward the isentrope. This is illustrated for Al in Fig. 8b. Thus, by carrying out a series of reflected experiments it is possible to extend the range of experimental conditions.

Another way to significantly modify the Hugoniot path is to start with a porous metal (Kormer et al., 1962). In porous matter solid particles are separated by empty spaces so that the average density is $\rho_{00} = \rho_0/m$ where m is the degree of porosity. The initial compression, from ρ_{00} to ρ_0, occurs at negligible pressure and is accompanied by a considerable heating and a rapid rise in temperature. At very high porosities such as are possible with fine metal powders, heating may be sufficient to lead to an expanded Hugoniot state. In the case of porous W, temperatures as high as 32,000 K at 2 Mbar have been reached in the 20% expanded metal (Krupnikov et al., 1962).

Shock-wave measurements have been carried out on most elements and on a very large number of compounds. The highest measured pressures have been obtained by L. V. Al'tshuler and coworkers at the Institute of Chemical Physics in the U.S.S.R. They developed an explosively driven system which achieved pressures of about 10 Mbar in high density materials like Mo and Ta, and 13.4 Mbar in Fe. Although most of this work was published between 1958 and 1968, Al'tshuler (1965) writes that, "In the main, these investigations (below 5 Mbar) were performed in 1948-1950." The Soviet work of several decades ago has proven to be quite accurate, although little in the way of a detailed description of their experimental configuration has been published. The most extensive single source of all published Hugoniot data up to 1977 is in the LLNL Compendium of Shock Wave Data (van Thiel et al., 1977). Marsh

(1980) has made available all of the Los Alamos data including previously unreported measurements. These two collections include data for elements, alloys, rocks, minerals and compounds, plastics and synthetics, woods, assorted liquids, aqueous solutions, and high explosives. Al'tshuler et al. (1981a) have reported a critical analysis of shock measurements for most of the metals and report best-fit U_s-U_p functions.

The large increase in temperature under shock compression is often an undesirable feature, and the possibility of a method resulting in only a small temperature rise is attractive. The principle of isentropic generation rests on dividing a single strong shock into a series of lower-amplitude shocks acting in sequence. No such technique exists, but a promising method under development involves the use of a gun-impact facility of the type traditionally used in shock-wave experiments, in which a flat-nosed projectile is launched at high velocity into a flat-plate target (Barker and Scott, 1984). A very special thin layer of variable density material is carried on the projectile nose-piece to cushion the impact and slow the rise-time of the input wave. No results have yet been reported.

2.3 Shock Temperature Measurements

Temperature cannot be determined directly from shock data, but must be obtained separately. Relatively few measurements have been made. The earliest studies, carried out in the U.S.S.R., have been summarized by Kormer (1968). More recently this work has been pursued by Lyzenga et al. (1979, 1982), and Ahrens et al. (1981) in a joint Caltech-Livermore program using the LLNL light-gas gun. Optical methods are the most suitable diagnostic techniques at the temperatures reached by shock-wave measurements. As a result, most of the work has been with transparent materials which permit the radiation emitted from a shock-front to pass through a layer of still-uncompressed matter (Fig. 6e). Some of the materials studied are alkali halides, simple liquids, quartz, and several intitially transparent minerals. The measured intensity versus wavelength of the emitted radiation is assumed to represent a gray or black body spectrum, and the temperature is determined by fitting these data to the Planck radiation formula.

The pioneering work of Kormer (1968) was concerned mainly with alkali halides. The brightness temperature of the shock-front was determined at two wavelengths (478 nm and 635 nm) by comparison with the radiance emitted by a

standard source. An important result of these studies was the determination of the high-pressure melting curve. Melting has little effect on the Hugoniot unless a change in chemical bonding occurs. But Hugoniot temperatures are strongly modified by melting. When a substance melts at atmospheric pressure, the added energy does not lead to a rise in temperature until the process has been completed. Under shock-compression, the pressure-temperature path passes through the melting curve as illustrated by the data for KCl (Fig. 9). Measurements have been made for NaCl, KBr, CsBr and LiF (Kormer, 1968) and recently for CsI (Radousky et al., 1984). The melting pressures range from 250 kbar for CsI to 2.8 Mbar for LiF, and temperatures range from 3000 K to 6000 K. Subsequent investigations by Kormer et al. (1969) at higher pressures discovered large systematic discrepancies between the measured and theoretical temperature values above 6000 K. Zel'dovich et al. (1969) attribute this to nonequilibrium processes in the emitting region arising from the finite time required to transfer electrons to the conduction band.

Temperature measurements are based on the assumption that the emitted radiation is in thermodynamic equilibrium with the compressed matter. Also, the shock-front through which this radiation must pass on its way to the pyrometer is optically thin (i.e., does not absorb). As we have seen, the first assumption has been challenged in the case of the alkali halides at very high pressures and temperatures. It also appears that one or both of these assumptions may also fail in a number of other cases for which temperature has been calculated and measured. For H_2O (Lyzenga et al., 1982), Ar, N_2 (Voskoboinikov et al., 1979), and C_6H_6 (Nellis et al., 1984b) the measurements are consistently below the predicted values and suggest a systematic discrepancy in either theory or measurements.

2.4 Melting Measurements above 1 Mbar

Melting along the Hugoniot of Fe, Al and Ta has been detected by measuring the sound velocity, a sensitive indicator of the loss in shear-strength from solid to liquid (Asay and Hayes, 1975; Brown and McQueen, 1980; 1982; Shaner et al., 1984). When a shock wave travels back into the impactor (Fig. 6f), it reflects off the rear impactor surface and returns toward the sample as an isentropic release wave (or catch-up wave) moving at the sound speed of the compressed material. This speed is generally higher than the shock speed and, if the impactor is sufficiently thin, the release

wave will catch and attenuate the shock. A measurement of the time and location of the attenuation leads to a determination of the sound speed. Plotted in Fig. 10 are measurements for Fe along with the calculated bulk sound velocities. The drop at 2 Mbar signifies the transition from ε to γ Fe; the second discontinuity, at 2.5 Mbar and a calculated temperature of about 5500 to 6000 K, is believed to be due to melting. Ta has been observed to melt along the Hugoniot near 2.95 Mbar and data for the Al alloy 2024 suggests this occurs at 1.3 Mbar (Shaner et al., 1983) and about 4800 K. The melting temperatures have been estimated from theory and are dependent on the model used. Unlike the alkali halides, metals have not been subjected to shock-temperature measurements because radiation passing from the shock front is absorbed by the unshocked matter. It may be possible to obtain temperature measurements by recording the emission from the shock-front when it reaches the sample surface.

2.5 Optical and Electrical Properties

A wide class of materials have been measured for optical and electrical properties (Davison and Graham, 1979), although considerably fewer than for thermodynamic properties. These studies provide information about the microscopic nature of the shocked state. The earliest optical studies measured the index of refraction (n) of transparent materials (Kormer, 1968). When the compressed material remains transparent, light is reflected off the shock-front, making it possible to determine n by recording the reflection angle and using Fresnel's equations of electromagnetic wave propagation. The index-of-refraction studies were initiated to provide information about the reflectivity and emissivity of shock-fronts, needed for temperature determinations. In general, n increases with density and in several cases, such as CCl_4 and C_6H_6, anomalously high reflectivities have been associated with chemical decomposition (Yakusheva et al., 1971 and 1977).

Recently there have been several spectroscopic studies of the shock front using Raman, stimulated Raman, and stimulated Brillouin scattering techniques. Bloom and Keeler (1974) demonstrated that stimulated Brillouin scattering can be used to measure sound velocity in shock-compressed fluids with 1% precision. They made measurements for H_2O up to 15 kbar. Holmes et al. (1983), using Raman scattering, determined the OH-stretching frequency in H_2O shocked to 70 kbar and a temperature of ~370 °C. They observed the

band-width to narrow, and suggest that this may be due to the breaking of weak hydrogen bonds between H_2O molecules. Backward-stimulated Raman scattering in shock-compressed C_6H_6 has been used to measure the frequency shift of the 922-cm^{-1} vibrational ring-stretching mode to pressures of 12 kbar (Schmidt et al., 1983).

Styris and Duvall (1970) have reviewed the literature on electrical conductivity through 1969. Davison and Graham (1979) noted that "most of the work is fragmentary and largely exploratory." Two exceptions are the measurements for H_2O and NH_3. Hamann and Linton (1969) first measured electrical conductivities in shock-compressed water and concentrated salt solutions up to 133 kbar (1.7 g/cm^3) and 1100 K. Recently Mitchell et al. (1982) extended these measurements to 590 kbar and 4200 K. Above 200 kbar the conductivity becomes constant at about 20 to 30 $(\Omega\ cm)^{-1}$ (Fig. 11). Clearly the processes leading to conductivity (molecular ionization) have become fully saturated. Hamann and Linton predicted this from an analysis of their lower pressure data. They concluded that above 150 to 200 kbar H_2O becomes fully ionized to H_3O^+ and OH^- and is then essentially a molten salt. Kovel (1973), measured the Hugoniot behavior and electrical conductivity of liquid NH_3 in the pressure range 45 to 282 kbar, with temperatures from 600 to 2300 K and he found results similar to those for H_2O.

2.6 X-ray Measurements

Flash x-ray diffraction is well suited to study atomic arrangements of crystalline materials during the very short passage-times of a shock front. An important question to resolve is whether shock-compressed material is isotropically compressed or strained in some direction (and therefore non-hydrostatic). Johnson et al. (1980) have used an intense 80-ns x-ray pulse to probe shock-compressed LiF crystals oriented in the [100] and [111] directions. A Ta projectile impacts an Al target and generates a shock in the sample. The camera records the shift in the Bragg angle of the reflected x-ray pulse, making it possible to determine the interplanar distances for the two orientations. The most crucial part of the experiment is to synchronize the x-ray pulse with the shock arrival at the surface. Experiments were conducted at pressures between 0.4 and 1.1 Mbar. The densities determined for the two orientations were within 1% of those calculated from the measured

shock- and particle-velocities using the Rankine-Hugoniot conditions (Johnson and Mitchell, 1980). This demonstrates that, for these crystals at least, crystalline order is maintained behind the shock front. In addition, these studies showed that LiF does not undergo a NaCl → CsCl phase change below 1.1 Mbar; that LiF does not appear to melt below 1.1 Mbar shock pressure; and that shock-wave compression does not immediately turn a single crystal of LiF into a powder or an amorphous mass. Temperature measurements had already shown that LiF melts along the Hugoniot at 2.8 Mbar (Kormer, 1968).

In the case of Al there is evidence to suggest that a state of uniaxial strain exists in the shocked solid. An x-ray diffraction study to 0.23 Mbar has determined differences in the lattice parameters along the [111] and [200] directions, suggesting the existence of strain inhomogeneities (Al'tshuler et al., 1981b).

2.7 Nuclear-Explosive-Driven Shock Compression

The pressures attainable in dynamic-impact experiments using conventional drivers, such as chemical explosives and guns, are currently limited to pressures between 1 Mbar for liquids and about 10 Mbar for dense metals. Higher pressures can be obtained using nuclear explosives and large lasers. In these experiments the shock velocity can be measured, but the mass velocity (U_p) must be obtained from theory. As a result, accurate experimentally determined standards do not exist in the pressure range above 10 Mbar.

The earliest work using nuclear explosives was reported by Al'tshuler et al. (1968b) in the U.S.S.R. They recorded the shock velocity as the shock passed through layers of investigated material such as Pb-Fe, Pb-Cu, Cu-Cd, SiO_2-Al and several other pairs (Trunin et al., 1969, 1972; Podurets et al., 1972). By determining a theoretical standard for one substance, such as Pb or Fe, comparative pressures and densities can be assigned to all other samples by using the impedance-matching method. Thomas-Fermi and Thomas-Fermi-corrected (TFC) statistical theories were used to calculate Hugoniots above ~300 Mbar, joined by interpolation with experimental results below 10 Mbar to determine a standard Hugoniot curve in the intermediate region (Al'tshuler et al., 1977). Pressures and densities were estimated to be in the range between 20 and 50 Mbar.

Ragan (1977) attempted to measure the mass velocity (U_p) in Mo by using the neutrons generated in a nuclear explosion as probes to determine the

Doppler-shifted resonance in a moving Mo baseplate. Neutrons from the explosion heat a uranium slab to 50 eV and the following expansion compresses the lucite and drives a shock-wave into the Mo (Fig. 12). Doppler-shifted neutrons provide the U_p of Mo. These measurements provided a single Hugoniot point at 20 ($\pm$ 2) Mbar. But the accurate determination of the entire Mo Hugoniot relies on a theoretical model calculation. In subsequent experiments (Ragan, 1980, 1982, 1984), a number of metals and compounds were shock-compressed to between 20 and 70 Mbar, and their pressures determined by impedance-matching with Mo as a reference, much as in standard shock experiments.

Avrorin et al. (1980) and Volkov et al. (1980) report having shock compressed Pb (158 Mbar), SiO_2 (70 Mbar), Al (55 Mbar) and H_2O (32 Mbar) using an impedance-matching method with an iron baseplate at 120 Mbar. They used a theoretical Fe standard based on TFC theory. The account of their work is brief and does not assign corresponding densities. Experiments employing nuclear explosives have been initiated at LLNL using Al as a theoretical standard (Nellis, 1984).

Some of the results of nuclear-explosive-driven experiments for Al have been collected in Fig. 13 and compared with theoretical calculations. Near 25 Mbar contributions from thermal electron, nuclear motion, and the 0 K pressure are of roughly equal magnitude. At this pressure the thermal energy (kT) is about one-half the Fermi energy, and the conduction band is a partially degenerate.

3.0 Condensed Matter

In principle, the equation of state and the properties of matter at high pressures can be determined from theory. In practice, the barriers to ab-initio calculations are formidable owing to the computational difficulty of solving the many-body problem. Consequently, it has proven necessary to introduce simplifying approximations into the governing equations. The price of simplification, however, is typically a loss of generality, and the resulting theory is adequate over only a limited region of the phase diagram. Some older well-known examples are the Thomas-Fermi model of dense matter and the van der Waals model of liquid critical phenomena. Each of these contains certain features essential for characterizing the material properties over a limited range of conditions. Bushman and Fortov (1983) and Godwal et al. (1983) have recently reviewed the subject of equation-of-state models.

In this section we review the high-pressure behavior of condensed matter for conditions in which the nuclear motion is roughly constrained or solid-like. The most important recent advance for condensed matter-theory has been the widespread usage of electron band theory. Although this theory has been understood for over 30 years, the explosive advance in computer technology and software development have now made sophisticated applications possible.

3.1 Electron Band Theory

We begin with the Hartree-Fock method and demonstrate its relationship to a hierarchy of less rigorous, but more widely-used, electron band theory and statistical models. Electron band theory yields techniques for solving the Schrödinger equation in a periodic potential. This topic has been recently reviewed by Koelling (1981). The various methods differ chiefly in their choice of basis functions, boundary conditions and approximations to the electron exchange and correlation. The Hartree-Fock equations are obtained by writing the trial wave-function as a Slater determinant of one-electron wave functions. In this approximation each electron moves in the field of the remaining N - 1 electrons, neglecting electron correlations other than exchange. For the ground state the total energy E is

$$E = T_e + T_i + U_{ee} + U_{en} + U_{ex} + U_{nn} \qquad (3.1)$$

where T_e and T_i are the electron and ion kinetic energies, and the remaining terms are respectively the electron-electron, electron-nucleus, electron exchange, and nuclear-nuclear energies. The proper solution is obtained by minimizing E with respect to the complete set of one-electron wave-functions. The procedure yields N different electron eigenvalue equations, each of which contains complicated multicentered exchange integrals in U_{ex}. The evaluation of the exchange term is cumbersome and demands a considerable amount of computer time.

Self-consistent solutions of the Hartree-Fock equations are greatly simplified if the exact exchange is replaced with a local free electron

approximation (Slater, 1951; 1979). The total exchange energy is written as

$$U_{ex} = -\frac{9}{4} e^2 \alpha \left(\frac{3}{8\pi}\right)^{1/3} \int \rho(r)^{4/3} dV \qquad (3.2)$$

where $\alpha = 2/3$ and $\rho(r)$ is the charge density. Correlation energy, U_{corr}, may also be added to Eq. (3.1) as a local density function approximation (Hedin-Lunqvist, 1971). The correlation energy is typically about 10% of the exchange energy and may be approximated by adjusting α (X-α method). Correlation is important at normal density where it controls the balance between positive and negative pressure contributions. Hohenberg and Kohn (1964) demonstrated that the proper value of $\rho(r)$ is the one that minimizes the total energy. This leads to one-electron Schrödinger equations in which the potential field is the same for each electron

$$\left(\frac{-\hbar^2}{2m} \nabla^2 + V(r) + \frac{d(U_{ex}+U_{corr})}{d\rho} \right) \phi_i = \epsilon_i \phi_i; \quad i = 1, 2 \ldots N, \qquad (3.3)$$

where ϵ is the energy of the ith electron and V(r) is the electrostatic potential. The pressure may be obtained using the virial theorem

$$PV = \frac{2}{3} \text{(Kinetic Energy)} + \frac{1}{3} \text{(Potential Energy)} \qquad (3.4)$$

In general the local density approximation works surprisingly well for solids and even for free atoms and small molecules, using only a small fraction of the computer time required by Hartree-Fock. It predicts energies of atomic ground and low-lying excited states more accurately than Hartree-Fock. For example, in an extensive set of self-consistent field calculations Moruzzi et al. (1978) demonstrated that electron band calculations can accurately describe the lattice constant, cohesive energy and compressibility of the full range of metals, given only the atomic number. A book reviewing density functional theory and several of its applications has recently appeared (Lundqvist and March, 1983).

Computer programs employing the local density functional method are now generally available. Among these are the muffin-tin methods (Slater, 1965; 1979), the augmented-plane-wave (APW) and Korringer-Kohn-Rostoker (KKR) methods, and the newer very fast versions such as linearized APW (LAPW), linear-muffin-tin-orbitals (LMTO), and augmented-spherical-wave (ASW) (see

Koelling, 1981). Skriver (1984) has written a book on the LMTO method which includes computer program listings. The newer methods are from ten to one hundred times faster and suffer only a slight loss in accuracy. They have had a great impact on high-pressure theory. In particular, their great speed allows for the calculation of a very large number of points in the Brillouin zone and therefore for very high precision in the total energy. This has made it possible to calculate high-pressure phase-transformations (see Sec. 3.4) which require very accurately determined energy differences.

A strikingly successful method for calculating static structural properties, crystal stability, and phase transformations has been developed in a series of papers by Cohen and coworkers (see for example Yin and Cohen, 1982a, b) in which they use a self-consistent pseudopotential method within the local density formalism. A non-local pseudopotential is used to represent the valence electron-core interaction. It is chosen to reproduce the corresponding all-electron excitation energies and eigenvalue- and wave-functions for electrons outside the core region. A plane-wave basis set is used to represent the (pseudo-) valence wave functions. By not explicitly including core-states, the calculated total energies are usually two orders of magnitude smaller than those associated with all-electron calculations. Hence the available computational precision permits an accurate resolution of total energy differences between structures. This accuracy is further enhanced by using the same pseudopotential for all structures. Calculations for Si and Ge predict the cubic diamond structure will transform to a metallic β-tin phase at 99 kbar and 96 kbar respectively (Yin and Cohen, 1982a, b). The corresponding experimental values are 125 kbar and 100 kbar. The results for carbon are particularly interesting because from among the fcc, bcc, hcp, sc and β-tin structures, the diamond phase is expected to be stable until 23 Mbar when it will transform to the simple cubic structure (Yin and Cohen, 1983). These authors believe that if diamond does transform to some other metallic phase, it will be at a pressure of at least 10 Mbar. The method has been applied to calculate the high-pressure phases of III-V semiconductors (Froyen and Cohen, 1983), alkali halides (Froyen and Cohen, 1984) and the simple metals Be (Lam et al., 1983) and Al (Lam and Cohen, 1981). A comparison of the self-consistent pseudopotential and LMTO methods has been made for the calculation of phase stability in Si (McMahan et al., 1981). LMTO calculations were made with all electrons, including the core treated

self-consistently and also with the core replaced by the same pseudopotential used by Yin and Cohen. The lattice-energy differences obtained by the three methods are found to be in millirydberg quantitative agreement.

3.2 Statistical Atom Models

Thomas-Fermi statistical atom models are the best known extreme-density theories and are often synonymous with the subject (March, 1957; Kirzhnitz et al., 1976). These may be derived from Eq. (3.1) by introducing a local-density free-electron approximation for the kinetic energy as well as for exchange and correlation. This further simplifies the numerical solution, but removes any vestige of the quantum shell structure. According to the density functional formalism, the replacement of the quantum mechanical kinetic energy by its statistical analog should be carried out as an expansion in $\nabla\rho(r)$ and leads to (Kalitkin and Kuz'mina, 1972; Perrot, 1979; and More, 1979)

$$E = C_k \int \rho^{5/3} dV + \frac{1}{72} \int \left|\frac{\nabla\rho}{\rho}\right|^2 \rho dv + U_{en} + U_{ee} + U_{ex} + U_{corr} \quad (3.5)$$

where $C_k = \frac{3h^2}{10m}\left(\frac{3}{8\pi}\right)^{2/3}$. Von Weizsäcker (1935) was the first to introduce the gradient term, although his was larger by a factor of nine. This theory is referred to here as TFDW. This term has the virtue of preventing a large electron density near the nucleus. Statistical theories are generalized to finite temperatures by replacing $\rho(r)$ with the Fermi distribution function (Feynman et al., 1949; Latter, 1955). The requirement that E be minimized with respect to variations in the electron density is subject to the condition that the number of electrons N remains fixed and leads to an integral equation from which the local charge-density may be obtained.

$$\frac{5}{3} C_k \rho(r)^{2/3} + \frac{1}{72}\left|\frac{\nabla\rho}{\rho}\right|^2 - \frac{1}{36}\frac{\nabla\rho}{\rho} + V(r) - \frac{d(U_{ex}+U_{corr})}{d\rho} = \mu \,, \quad (3.6)$$

This is the statistical model analog of the one-electron Schrödinger Equation (3.3) where μ, the chemical potential, replaces the one-electron eigenvalue.

The neglect of the gradient term and correlation energy leads to the Thomas-Fermi-Dirac (TFD) theory (Cowan and Ashkin, 1957), and the additional

neglect of exchange leads to the Thomas-Fermi (TF) model (Latter, 1956). The great virtue of TF is that all its properties scale with Z, and a single set of calculations at all densities for one Z suffices for all Z's. This feature is not present in the other statistical models. The TFC theory (Kalitkin, 1960) is an attempt to include more physics in TF while retaining its advantageous scaling features by using the TF charge densities (ρ_{TF}) to approximate ρ.

Figure 14 compares the experimental zero-pressure atomic volumes with those calculated by electron band theory and several statistical models. The obvious failure of any statistical model to properly characterize the main features of the periodic table is due to the omission of atomic structure. Instead each model is fortuitously best for a different group of elements. Kirzhnitz and Shpatakovskaya (1972) have attempted to introduce atomic structure or "oscillations" into the Thomas-Fermi model. It appeared to be a promising way to include quantum mechanics while retaining the basic numerical simplicity of a semi-classical model. Unfortunately, the model predicts a series of unrealistic phase-transitions at densities for which different shells are squeezed into the continuum (Kirzhnitz et al., 1976).

Statistical models are expected to be most reliable at extreme conditions when the detailed influence of electronic structure has been obliterated. Despite the omission of quantum structure, statistical models typically predict electronic densities that are a good average of the exact results. As the pressure or temperature is raised, successive shells of electrons are delocalized. These effects exhibit themselves as wiggles in the equation of state that are represented only in an averaged manner by statistical models. In Fig. 15a the curvature in the band-theory results for Li arises from the delocalization (pressure ionization) of the 1s core levels. Although the TFD model shows no such behavior, it does represent a good average. Above 600 Mbar both models are in agreement. Similar results have been observed for Al (McMahan and Ross, 1979). The same features appear in the high-temperature Li plasma (Fig. 15b) where the stepped features exhibited by the Saha model result from successive electron ionizations, while the TF and TFC theories demonstrate a smoothed behavior (Iosilevskii and Gryaznov, 1981). At higher densities this structure disappears because the discrete atomic levels become pressure-ionized and broadened into bands.

3.3 Thermal Properties

Thermal contributions to the equation of state may be included by neglecting electron-phonon interactions and separately adding the uncoupled electronic (ΔE_e) and nuclear motion (ΔE_n) contributions to the ground state properties (E_0),

$$E(V,T) = E_0(V) + \Delta E_e(V,T) + \Delta E_n(V,T) , \tag{3.7a}$$

$$P(V,T) = P_0(V) + \Delta P_e(V,T) + \Delta P_n(V,T) . \tag{3.7b}$$

ΔE_e and ΔP_e can be obtained from finite-temperature self-consistent band calculations for electrons in a rigid lattice, using Fermi statistics to determine the energy level occupation numbers (McMahan and Ross, 1977; Liberman, 1979; Voripinov et al., 1970). For $T < T_F$ the results of such calculations can be very well approximated by a simple model based only on ground-state electronic properties. Accordingly,

$$\Delta E_e(V,T) = \sum_i \epsilon_i(V)[n_i(T) - n_i(0)] , \tag{3.8a}$$

$$\Delta P_e(V,T) = -\sum_i \frac{d\epsilon_i(V)}{dV} [n_i(T) - n_i(0)] , \tag{3.8b}$$

where $\epsilon_i(V)$ are the ground-state eigenvalues obtained from the same band calculations used to generate $E_0(V)$ and $P_0(V)$, and $n_i(T)$ is given by the Fermi-Dirac distribution function.

If the interatomic potential is known, then the nuclear motion terms can be determined directly. With the exception of simple metals and closed-shell atoms, this procedure is generally not possible. Instead, it is necessary to introduce approximations which bypass a knowledge of the microscopic physics and rely on macroscopic variables -- the pressure-volume curve to obtain nuclear thermal properties via the well-known Grüneisen model,

$$\Delta P_n = \frac{3\gamma RT}{V} , \quad \text{and } \Delta E_n = 3RT , \tag{3.9}$$

where γ is the Grüneisen parameter. Several useful approximations for γ can all be expressed in a single equation:

$$\gamma = -\frac{V}{2}\frac{\partial^2 (P_0 V^{2m/3})/\partial^2 V}{\partial (P_0 V^{2m/3})/\partial V} + \frac{1}{3}(m - 2) , \qquad (3.10)$$

where $m = 0$ is for an elastic continuum model (Slater, 1939), $m = 1$ is obtained from a harmonic expansion of the static lattice energy (Dugdale-MacDonald, 1953; Rice et al., 1958), and $m = 2$ is based on the harmonic vibration of an atom in the spherically symmetric field of neighbors (Zubarev and Vashchenko, 1963). A number of useful empirical relations have been offered which bypass these models. These assume γ/V = constant, or $\gamma = CV + 1/2$, where C is a constant fitted at normal density. $\gamma = 1/2$ is the limiting case at $T = 0$, and $V \to 0$ for a lattice of positive ions in a degenerate electron gas. In the limit of $T \to \infty$, $\gamma \to 2/3$. The Hugoniot curve may be calculated using Eqs. (3.7) to (3.10) to solve Eq. (2.3). A more common procedure has been to reduce the shock data to isotherms. Zharkov and Kalinin (1971) have written a comprehensive review of shock-reduction methods and their results.

A serious deficiency of the Grüneisen model is that it does not properly describe the fluid state often attained at high shock-temperatures. In the case of simple metals such as the alkalis, aluminum, etc., an effective ion-ion interaction can be determined and with the use of liquid perturbation theory and thermal properties, melting curves and Hugoniots may be calculated (Godwal et al., 1981; Ross, 1980; Young and Ross, 1984). The theory of liquid simple metals has been extensively reviewed (Ashcroft and Stroud, 1978) and only its essential features are summarized here. The liquid is approximated by a system of hard-sphere ions in a neutralizing nearly free electron fluid. An electron-ion interaction is constructed using pseudopotential theory. This leads to a piling up of electrons around the ions and to a dielectric-screened ion-ion interaction (V_{I-I}). The Helmholtz free energy is expressed (schematically) as

$$A \leq A_{eg} + A_{HS} + \frac{N}{2}\int V_{I-I}(r)\, g_{HS}(r,d)\, dv \quad . \qquad (3.11)$$

The contributions are, respectively, from the free electron gas, hard spheres of diameter d, and an interaction term which includes the hard-sphere pair distribution function. The correct value of d is the value that minimizes the right hand side. Pressure and energy are obtained by numerical differentiation. By using Fermi-Dirac statistics the theory is generalized to

include thermal electronic excitation. This model was used to calculate the aluminum Hugoniot in Fig. 13. Here the ion-ion potential was determined by fitting the 0 K solid version of the theory to an LMTO isotherm up to 25 Mbar using a local electron-ion pseudopotential screened by the Hubbard dielectric constant.

Kerley (1983) has developed a theory for dense liquids that does not require explicit knowledge of the intermolecular potentials. Instead, the potential energy of the fluid is calculated from the 0 K solid isotherm. Since this curve is often known from theory or experiment, the model (PANDA) can be applied to many practical problems (Kerley, 1981). The Los Alamos National Laboratory has created the SESAME library of equation of state tables for approximately 30 different materials which cover a wide range of temperatures and densities (Bennett et al., 1978). The library is available on request.

3.4 Electronic Transitions and Phase Stability in Metals

It is now recognized that many of the interesting high-pressure phenomena, such as electronic and structural phase-transitions, metallization, and irregularities in the equation of state, can be understood in terms of systematic changes with compression in the electronic structure. For a review of some of the earlier work see Drickamer and Frank (1973). In metals, valence d electrons are relatively localized, compared to s and f electrons, and have comparable energies. The d electrons are typically closer to the nucleus so that, on compression, s electrons transfer into d states at very little cost in energy but causing large changes in the compressibility. The f electrons are typically localized and, except for the early actinides, they play no role in bonding. Under sufficient pressure they may undergo a Mott transition and become delocalized. By changing the lattice parameter electrons may be transferred between states and, in effect, transform elements into approximations of their neighbors. This feature, dubbed "pressure tuning," has proved useful for understanding materials at ambient conditions.

3.4.1 sp→d Transitions

The role played by d-electron states is dramatically illustrated by the behavior of Cs and Xe. Cs metal at room temperature undergoes an isostructural electronic transition (fcc-fcc) at 42.2 kbar with a 9% volume

change (Bridgman, 1948; Jayaraman et al., 1967). Sternheimer (1950), on the basis of Wigner-Seitz calculations, showed that at normal density the highest occupied band was 6s-like and the lowest unoccupied levels were 5d-like (Fig. 16). nder compression, the empty d-like states decrease in energy relative to the s-like, crossing the Fermi level near the density of the observed transition. This suggests that the high compressibility and the isomorphic transition results from the promotion of s-like electrons into the empty d-like levels. These results are basically correct, but oversimplified because they neglect mixing (hybridization) of s- and d-like states. At even higher compression, the bottom of the Cs valence band drops below the top of the 5p "core band," and closes, making some 5d and 5p states become degenerate. For Xe, APW band calculations predict this same gap-closure will lead to metallization at about 1.3 Mbar (Ross and McMahan, 1980; Ray et al., 1981). The negative volume derivatives of these electron energy levels may be roughly viewed as electron partial pressures. Thus, the 5d electrons have lower partial pressures than do either the 5p or 6s electrons. As a result, an electron transferred into a 5d state, either by thermal excitation (as in shock-compressed Xe) or static-compression (Cs), leads to a decrease in that electron's contribution to the total pressure, and will be observed as a softening of the pressure-volume curve.

Experimental evidence (McWhan et al., 1974) indicates that, as a result of s-d hydbridization, the transition in Cs is more complicated than the simple picture, and in fact the shift in electrons is continuous over a range from 0 to 100 kbar. Glötzel and McMahan (1979) suggested, on the basis of a relativistic electron band (LMTO) calculation and a simple model of the thermal properties, that a possible mechanism for the observed transition is an anomaly in the lattice vibrational contribution to the pressure which is connected with the s→d transfer. The first effect of the s→d transition is the softening in P_0 that accompanies the transfer of electrons. The second effect manifests itself through the lattice vibrational properties. In the case of Cs, the softening in P_0 is sufficient to create a negative γ. This translates into a negative contribution to the thermal pressure and a van der Waals loop implying a first-order isostructural phase-transition, as observed (Fig. 17). At higher pressures, where the transition is largely complete, there is additional stiffening due to overlap of the 5p cores. The Grüneisen parameter (γ) has recently been measured in solid Cs to 43 kbar at

22° C, and in liquid Cs to 20 kbar at 200° C (Boehler and Ross, 1984). The results show a sharp drop in γ near 42 kbar, in agreement with Glötzel and McMahan.

Rb and K behave similarly to Cs. They undergo bcc-fcc transitions at 700 and 1100 kbar respectively and structural transitions at pressures up to 2000 kbar (Takemura and Syassen, 1983; Olinyk and Holzapfel, 1984). Although no evidence exists for an isostructural transition in these elements, the near-infrared reflectivity studies provide evidence for a pressure-induced 5s → 4d transition in Rb, and 4s → 3d transition in K (Takemura and Syassen, 1983; Tups et al., 1983).

Although the maximum compressions achieved with shock-wave experiments on liquid Xe have been insufficient to achieve metallization, the high temperatures attained, up to 30,000 K, are sufficient to transfer a considerable number of electrons into the empty 5d level (Ross, 1968; Ross and McMahan, 1980). The extent to which thermal excitations modify the observed pressure-volume Hugoniot curve depends on the electron band gap and its volume derivatives. Figure 18 is a comparison of theoretical and experimental results (Nellis et al., 1982). Curves A and B are Hugoniots calculated using fluid theory for two slightly different volume-dependent band gaps obtained from APW band theory. Calculations that do not include electronic excitation, the pure insulator case, are shown by the uppermost curve (C). By absorbing some of the shock energy, the excited electrons act as thermal sinks, keeping the temperature down and lowering the pressure. The volume dependence of the energy gap also plays an important role. Because the 5p-5d gap is narrowing with decreasing volume, electrons excited from 5p to 5d undergo a decrease in their partial pressures, lowering the pressure further. The thermal excitation of core electrons to d levels has also been observed in liquid Ar shock-compressed to 910 kbar and about 26,000 K (Ross et al., 1979). The (sp→d) transition is now recognized to be a ubiquitous property of substances with available unfilled d states.

Evidence for the s-d transition has been observed in the shock-wave data for the heavy alkali and alkaline earth metals, and for the early transition elements (Fig. 19) (Al'tshuler et al., 1968; 1969). The middle and late transition elements are primarily d-electron-like at normal density, and any additional pressure-induced shifts are barely discernable. Detailed calculations for fcc La $(sd)^3$ show that even at P = 0, about two of the

three valence electrons are already in d states, so the transition is less dramatic than in Cs (McMahan et al., 1981). Nevertheless the effects are observable. The principal cause of the anomaly in La is the termination of the soft 6s-5d transition and some repulsion between rare-gas cores.

An extreme example of the s-d transition reports that Ni should transform from a metal to an insulator at a pressure of 340 Mbar (an eight-fold compression) and then revert back to a metal at 510 Mbar (Gandelman et al., 1963; McMahan and Albers, 1982). The metal-to-insulator transition occurs when the bottom of the partially filled s-band rises above the Fermi surface leaving a filled $3d^{10}$. At higher compressions the 3d and empty 4f overlap and close the insulating gap.

3.4.2 Structural Stability of s-d Metals

Pettifor (1970, 1977), and Mackintosh and Anderson (1980) have shown that the sequence of structures observed across the transition metals is closely related to the d-band occupancy and can be predicted from band theory. Skriver (1982), using LMTO theory, also found that the sequence of structures observed in the alkaline earths hcp (Be, Mg), fcc (Ca, Sr), bcc (Ba, Ra), and early transition elements hcp (Sc, Y, La) are characterized by an increase in d character (n_d). Thus, a pressure-induced increase in n_d leads to this sequence and has been observed by Olinyk and Holzapfel (1984): Ca (fcc→bcc) at 195 kbar; Sr(fcc→bcc) at 35 kbar; and Ba (bcc→hcp) at 55 kbar. At still higher pressures, the alkaline earth metals enter more complicated structures than those so far considered.

In the rare earths, f electrons are well localized, play no role in bonding, and may be considered as part of the ion core. But calculations show that the degree of d-band occupancy (increasing from Tm to La) again determines the observed pressure-induced sequence of crystal structures (Duthie and Pettifor, 1977).

3.4.3 f-electron Systems

Elements with f electrons fall into one of two categories: rare earths and late actinides (starting with Am), in which the f-electrons are localized; and the early actinides (Pa-Pu), in which itinerant 5f electrons, strongly hybridized with 6d, 7s and 7p character, play the same role as conduction electrons in transition elements. Under sufficient pressure, any rare earth

or late actinide will undergo a transition from rare-earth-like to early-actinide-like behavior, characterized by a change in f-electron character from localized to itinerant. Evidence for the nature of this transition exists for Ce at 7.5 kbar (Johannson, 1977; Pickett et al., 1981), Pr at 210 kbar (Mao et al., 1981; Smith and Akella, 1982), Am at 110 kbar (Johannson et al., 1981), and Bk and Cf at 250 kbar and 410 kbar, respectively (Benedict et al., 1984).

Shock-wave studies (Fig. 20) show the existence of a high-pressure phase-transition in all members of the rare earth series (Al'tshuler et al., 1968, 1969; Gust and Royce, 1973; Carter et al., 1975). However, except for Ce and Pr, there is no evidence that the observed transition is an f-electron delocalization or an s-d transfer effect. In addition several other possibilities have been suggested. Gust and Royce interpret the abrupt stiffening in pressure to be evidence of the onset of interaction between closed inert-gas cores after the s-d transition with no f-electron participation. Carter et al. identify the transition with melting. This is unlikely because liquid and solid Hugoniots at melting typically differ by only a small density change, unless accompanied by a large change in coordination as in diamond. Alt'shuler et al. (1981c) argue on the basis of spherical cell Wigner-Seitz-type band-calculations that these shock transitions are due to an increase in the number of f electrons, at the expense of s electrons, as the result of a downward shift in the f band and an upward shift of the s band above the Fermi surface--in other words, an s→f transition. However, spherical cell calculations do not properly treat the crystal symmetry, and are known to give poor results for high angular momentum states.

The major obstacle facing satisfactory theoretical solution of f-electron delocalization is the proper treatment of the localized regime. Local-density functional band theory predicts good pressure-volume curves for the itinerant state, but fails in the localized state. Some improvement has been obtained using spin-polarized band calculations (Skriver, 1980; Johannson et al., 1981).

Anisichkin (1978) and Al'tshuler et al. (1981a) examined the data for metals and have shown that the initial slope of the U_s-U_p curve, a_1 in Eq. (2.4), is approximately related to the position of the elements in the periodic table. A histogram of the metals (Fig. 21) according to a_1 show that all substances have values between 0.6 and 1.6, and fall into three

groupings. The smaller the value of a_1 the larger the compressibility. The first grouping (at the left) contains mainly rare earths and early transition elements which undergo electronic transitions (see Figs. 19 and 20). In their high-pressure states these elements are characterized by a_1 values that are nearer the middle range. The middle group contains elements which do not undergo electronic transitions. They are mainly found on the upper left side and in the center of the periodic table and are characterized by a linear $U_s - U_p$ relation, rising slightly due to electronic excitations. In the third group the elements mainly occupy the right side of the periodic table. Overall there appears to be a leveling under compression in which elements tend toward the middle group. These observations are consistent with the view that extreme compression tends to wash out the details in atomic structure.

3.5 Metallization of Closed-Shell Insulators

In the isoelectronic sequence Xe, CsI and BaTe, and in related substances such as BaSe, KI, and RbI, metallization is believed to proceed with the bottom of the empty d-like band dropping in energy below the top of the filled p-like bands (Fig. 16). APW calculations predict that Xe will become metallic above 1.3 Mbar, at a volume very near the value of 10.2 cm^3/mole predicted by Herzfeld (1927). The predicted narrowing of the band gap is in very good agreement with DAC optical measurements to 550 kbar (Syassen, 1982; Asaumi et al., 1982). For the case of CsI, calculations (Aidun et al., 1984) and optical measurements (Knittle and Jeanloz, 1983; Makarenko et al., 1984) suggest that the insulator-to-metal transition occurs in the range 1.0 ± 0.1 Mbar. Asaumi (1984) estimates metallization to take place at 0.7 Mbar. Calculations of the CsI Hugoniot show that, as in the case of Xe (see Fig. 18), electrons excited thermally to the conduction band cause a significant softening of the Hugoniot (Aidun, et al., 1984). These results are consistent with the high electrical conductivity observed under shock loading (Gatilov and Kuleshova, 1981) and with the shock temperature measurements to 1 Mbar (Radousky, et al., 1984).

Herzfeld (1927) made one of the earliest predictions of metallization. He developed a model which predicted that a closed-shell atom or molecule would become a metal when the molar volume (V) became equal to, or less than, its gas-phase molar refractivity (R). $R = (4\pi/3)N\alpha$, where N is Avogadro's number and α is the atomic polarizability. The predictions of this simple

model have been shown to be in surprisingly good agreement with those of sophisticated band theory and available experimental data closed-shell systems (Ross, 1972; Ross and McMahan, 1981; and Jayaraman, 1983).

The similarity of the electronic configuration in Xe, CsI and BaTe reflects itself in the systematic trend shown in Fig. 22 where the measured optical gaps are plotted vs $\ln (v/v_H)$. Here v is the actual volume and v_H is the gap-closure volume predicted by the Herzfeld model. The pressure dependence of the fundamental-absorption edges in RbI and KI crystals has been investigated up to 0.7 Mbar. Metallization pressures are estimated to be 0.85 and 1.15 Mbar, respectively (Asaumi et al., 1983). Grzybowski and Ruoff (1984) report that BaTe exhibits band-overlap metallization at a pressure of 200 kbar, and a volume compression of 0.65, in good agreement with the Herzfeld model.

Solid iodine is one of the few molecules whose pressure-induced metallization has been carefully observed in the laboratory, and it is now recognized as a possible prototype for the metallization of hydrogen. Balchan and Drickamer (1961) were the first to discover that the electrical conductivity increased dramatically at 50 kbar until it reached a metallic value at 170 kbar. Over this range the optical gap decreases steadily and closes at the metallization pressure (Riggelman and Drickamer, 1963). DAC x-ray diffraction studies show that over this pressure range the intermolecular and intramolecular atom-atom distances approach each other continuously and, although the band-gap closes near 170 kbar, the crystal remains molecular up to 210 kbar. At this pressure it dissociates in a first-order transition into a monatomic lattice with a 4% volume change (Takemura et al., 1980). Above this pressure the low-energy optical reflectivity exhibits typically metallic free-electron-like behavior in which the reflectivity decreases with increasing photon energy. Above 1 eV the increasing reflectivity is attributed to 5p innerband transitions or to transitions from the 5p to the bottom of the empty 5d band (Syassen et al., 1981). This behavior is absent below 210 kbar. The overall picture is consistent with shock-wave data to 1.7 Mbar (Fig. 23), showing a continuous change from the initial molecular phase to a monatomic metal (McMahan et al., 1977) and eventually a softening in the metal-phase Hugoniot due to p→d transfer. Reflectivity measurements show evidence for a metallization transition in IBr above 240 kbar, but none for Br_2 up to 600 kbar (Syassen and Reichlen, 1984).

3.6 Hydrogen: High-Pressure Physics in a Capsule

As a consequence of its simplicity, its possible applications, and a fascination surrounding its metallic phase, hydrogen has been the focus of considerable activity (Ross and Shiskevish, 1977; Silvera, 1980). Theoretical studies predict that at sufficiently high pressures (commonly thought to be between 1 and 4 Mbar), molecular hydrogen should undergo a phase transition into a metallic state. Whether this transition will be similar to iodine, or be the result of a direct dissociation into an alkali-like metal remains a major question.

The potential usefulness of metallic hydrogen can be attributed to several factors. As a result of its predicted high Debye temperature (~2000 to 3000 K), Ashcroft (1968) speculated that it may be an elevated-temperature (possibly room temperature) superconductor. The high specific-impulse of metallic hydrogen makes it attractive as a potential rocket fuel. However, if the energy release rate is not controllable once the transition is initiated, the metal would be an explosive rather than a fuel. Several major problems have to be resolved before it can be determined whether metallic hydrogen can be produced in the laboratory and if it will be technologically useful. The most important and elusive questions are whether the transition will occur at a pressure that can be reached in a static press and, assuming it can, how long it will remain in the metallic state (i.e., its metastability). The prospects for making and studying metallic hydrogen were sufficiently attractive that a surge of interest developed shortly after the appearance of Ashcroft's paper. At present, the principal interest is purely scientific, with possible applications remaining as speculative as when they were first proposed.

Silvera (1980) and Driessen and Silvera (1984) have surveyed the properties of solid H_2 up to about 20 kbar. Nellis et al. (1983) and van Thiel et al. (1973) have carried out shock experiments with liquid D_2 (Fig. 8a) to about 800 kbar (T ~ 7000 K) and H_2 to 100 kbar (T ~ 3300 K), using two-stage guns. The explosive-driven shock measurements of Dick and Kerley (1980) extend to 70 kbar for liquid H_2 and 120 kbar for D_2. Pressure versus volume measurements made using the DAC have been reported by Shimizu et al. (1981) up to 200 kbar at 300 K and by van Straaten et al. (1981) up to 370 kbar at 5 K. The order-of-magnitude increase in pressure

over a short time span demonstrates the rapid advance in DAC technology. But the measurement of volume by the DAC method poses a special problem. In the DAC, density is generally obtained by x-ray crystallography which is not practicable in the case of H_2, and one must resort to other methods. Van Straaten et al. have obtained the volume by measuring the sample area photographically and determining its thickness by interferometric techniques. This procedure requires a separate measurement of the pressure dependence of the index of refraction.

Shimizu et al. measured the pressure dependence of the sound speed by Brillouin scattering and then obtained the density by integration. In both sets of measurements, the authors estimate the final density to be in error by about 6%. This is also the degree of uncertainty expected from the measurements and from reduction of the shock data. The data of van Straaten et al. (Fig. 24) are in excellent agreement with the shock data (in Fig. 8) reduced to a 5 K isotherm.

Raman-scattering studies have been used to examine the H-H and D-D stretching and rotational frequencies. The stretching frequency increases with pressure as expected, but levels off near 300 kbar and begins to decrease with increasing pressure up to 600 kbar (Sharma et al., 1980; Wijngaarden et al., 1982). The softening of the intramolecular bond may be related to an increase in the bonding between atoms of different molecules and may be a precursor of the metallic transition.

At very low temperatures and pressures, solid parahydrogen and orthodeuterium are in spherically symmetric (J = 0) states. Raich and Etters (1972) predicted that at sufficiently high density the anisotropic interactions would make the molecules align, and the essentially free molecular rotations would change to librations about equilibrium configurations. Silvera and Wijngarden (1981) have observed this to occur in orthodeuterium near 278 kbar at 5 K. The transition is preceded by a broadening of the rotational band between 200 and 278 kbar, due presumably to a mixing of higher J values into the J = 0 ground state. Above 278 kbar, the band splits when the spherically symmetric molecules enter the orientationally ordered state. In parahydrogen no transition has taken place up to 540 kbar.

Since the pioneering work of Wigner and Huntington (1935), a large number of metallization-pressure predictions have been made, representing a formidable challenge to any reviewer. These results are extremely sensitive

to the free energies, and small uncertainties lead to large differences in the predicted pressure. As a result, the predictions vary considerably but the distribution appears to peak around 3 Mbar (±1 Mbar). In the past a larger uncertainty had been in the determination of the molecular equation of state. But, given the recent experimental work, this may no longer be the case. Most theories such as APW, Wigner-Seitz, Hartree-Fock, and third-order-perturbation theory predict similar hydrogen equations of state (Ross and McMahan, 1976). The largest uncertainty may be in estimates of the electron correlation energy. Van Straaten et al. predicted transition pressures ranging from 1.9 to 3.6 Mbar using the extrapolation of their molecular isotherm and the results of several metallic models from Ross and McMahan.

The possibility exists that molecular H_2 may undergo the same continuous transition observed in iodine. Friedli and Ashcroft (1977) calculated the pressure dependence of the molecular band gap and predicted closure to occur at 2.4 cm^3/mole (~2.1 Mbar). At this pressure, molecular hydrogen would be conducting and would convert to a metal at a somewhat higher pressure. These predictions could be verified by DAC optical-gap measurements above 400 kbar, where the band gap is believed to drop below 4 eV. For a review of recent work on this topic see Wood and Ashcroft (1982).

A novel mechanism for lowering the metallization pressure has been suggested by Carlsson and Ashcroft (1983). They note that since the band-gap (Eg) drops with compression, a concentration of x electron-hole pairs is expected to decrease the pressure by $P^{e-h} = -x\partial Eg/\partial V$. These authors propose creating the electron-hole concentration with laser synchrotron radiation; they find that a 5% concentration could lower the transition pressure by 0.35 Mbar. But this effect will be at least partially cancelled by a pressure increase arising from the creation of much-larger-sized H_2^+ molecules.

The first suggestion that the metal could be metastable at low pressures came from Brovman et al. (1971, 1972). Their static-lattice calculations using third-order-perturbation theory predicted that highly anisotropic filametary structures of metallic hydrogen had a lower energy than the ordered cubic structures, representing a metastable phase which is dynamically stable at pressures close to zero. The implication is that a filametary metal could remain "stuck" in such a state and not convert to molecules. But a proper calculation for the stable structure of a quantum solid at 0 K must contain

zero-point motion included self-consistently; this calculation shows (Straus and Ashcroft, 1977) that the large zero-point oscillations favor the formation of isotropic or cubic structures.

Several researchers claim to have made metallic hydrogen (Grigorev et al., 1972, 1978; Vereshchagin et al., 1975; Hawke et al., 1978). However, none of these claims have achieved any significant degree of acceptance in the high-pressure research community largely because they do not present a well-documented transition-pressure measurement, or a clear determination of the nature of the transition. There is no question that molecular hydrogen will eventually become metallic.

4.0 Dense Fluids and Plasmas

Much of the recent work on dense fluids and plasmas can be organized according to the phase diagram shown in Fig. 25. Shock Hugoniot data for dense liquids have been obtained to pressures and calculated temperatures as high as several Mbar and several tens of thousands of Kelvin (Nellis, 1983). These results have provided important information about intermolecular forces and atomic and electronic processes at extreme conditions. Gases have been compressed using explosive shock tubes to achieve nonideal plasma states in Ar, Xe and Cs (Mintsev and Fortov, 1983). Hot expanded metals are intermediate between liquids and nonideal plasmas. This range is, at present, very difficult for theoretical and experimental study. Experiments require the combinatin of high temperature and pressure while studying materials in a reactive state. The principle impediment to theoretical calculations stems from a lack of understanding of the localized itinerant electronic transition: the Mott transition (Hensel, 1981).

The most important advances in the theory of fluids have come from computer simulations and computationally fast approximate models. For a number of well-defined potentials, simulations carried out by Monte Carlo and molecular dynamics methods have been used to determine the pair distribution, and thermodynamic and transport properties over a wide range of conditions. An extensive set of data exists for the hard sphere, Lennard-Jones, and inverse-power potentials.

Computer simulations should be viewed as experiments producing exact data which complements laboratory experiments. For the case of strongly coupled degenerate plasmas with densities comparable to those found in high-energy

astrophysics and laser-fusion-compression experiments, computer simulations are the only "experimental" data. Computer simulation results have been extremely valuable in the development and testing of approximate methods such as variational fluid theory and the hypernetted chain method. These methods are now "work horses" for applications to simple fluids and dense plasmas respectively. For a review of computer methods and results, see Barker and Henderson (1976), and Binder (1979). Although computer simulations provide a sound basis for statistical theories, they typically deal with idealized systems. The physically interesting atomic and electronic processes must be introduced separately with approximate models.

4.1 Shock-Compressed Liquids

Fluid-variational theories have proven very useful for analyzing shock data in terms of the fundamental physics. In variational theory, the Helmholtz free energy (A) is approximated using the inequality

$$A \leq A_0 + \frac{N_0}{2} \int (\phi(r) - \phi_0(r))\, g_0(r)\, d^3r \qquad (4.1)$$

This expression states that the free energy of the actual system (A) is bounded above by the free energy of the reference (A_0) plus the difference in the potential energy between the actual system and the reference system, averaged over all configurations of the reference. ϕ and ϕ_0 are the pair potential of the actual and reference systems, respectively, and g_0 is the pair distribution function of the reference. The properties of the reference system may be taken from computer simulation results. By employing hard spheres, molecules are approximated as "billiard balls" with an infinite repulsion for separations less than or equal to d, but interact through ϕ_{ij} for $r > d$. The value of the variational parameter d is chosen to be the one which minimizes A. Thermodynamic properties are computed numerically by taking the appropriate derivatives of the free energy (Mansoori-Canfield, 1969):

$$\beta P = -\left(\frac{\partial \beta A}{\partial v}\right)_T + 1 \qquad (4.2)$$

and

$$\beta E = \left(\frac{\beta \partial \beta A}{\partial \beta}\right)_V + \frac{3}{2} \qquad (4.3)$$

where $\beta = 1/kT$ and k is the Boltzmann constant.

A convenient feature of the hard-sphere system is that the reference free-energy and pair distribution function are known from computer simulations and may be expressed analytically (Barker and Henderson, 1976). In general, the use of hard spheres introduces repulsions that tend to be too stiff. This can be overcome by making the reference free-energy correspond to that of the softer inverse twelfth power potential. As a result the modified theory (soft-sphere theory) is more accurate for high-density shock-compressed fluids (Ross, 1979; 1980). Kerley (1980 a, b, c) has examined many of the fluids reviewed in this section using the CRIS model, obtaining similar findings.

Some of the methods used to calculate the intermolecular potential from first principles have been reviewed by Margenau and Kestner, (1971) and Torrens, (1972). Typically the forces calculated between pairs of molecules appear too stiff when used at high densities because they neglect many-body interactions. The case of H_2 illustrates this well. Figure 26 compares the H_2-H_2 pair-potential determined from quantum mechanical calculations (Ree and Bender, 1979) with that derived from shock data. A more satisfactory pair-potential fitting is to use solid-state electron band calculations which include many-body interactions. This has shown to be successful in the case of solid H_2 (Liberman, 1976) and He (Young et al., 1981).

In a series of papers, Gordon and his coworkers have developed an approximate a priori theoretical method for calculating the intermolecular forces in closed-shell systems. This method, based on the electron gas approximation, was first applied to rare gases (Kim and Gordon, 1974). It has recently been used to obtain high-pressure equations of state and structural transformations for ionic solids (see for example Boyer (1981), and LeSar and Gordon, (1982)). The model assumes that the total electron-density of a closed-shell solid can be expressed as the superposition of the constituent charge densities obtained from Hartree-Fock calculations. The total energy is calculated in the statistical atom, or "Thomas-Fermi," approximation. LeSar and Gordon (1983) have extended the theory to solid N_2 and CO_2, and their calculated isotherms are in good agreement with static measurements to 100 kbar.

For many dense liquids a useful semi-empirical potential is the Buckingham exponential six,

$$\phi(r) = \epsilon \left[\left(\frac{6}{\alpha-6}\right) \exp\left\{\alpha\left(1 - \frac{r}{r^*}\right)\right\} - \left(\frac{\alpha}{\alpha-6}\right)\left(\frac{r^*}{r}\right)^6\right] \qquad (4.4)$$

where α, r^* and ϵ are adjustable parameters, typically obtained by fitting to experimental data, which determine the repulsive stiffness, the position of the potential minimum and its depth. The exponential term is a more realistic characterization of interatomic repulsive forces than the inverse twelfth power (Lennard-Jones) potential. At very small separations the attraction may become unrealistically large. This can be avoided by multiplying the attractive term by a damping function.

4.1.1 Inert Gases

Liquid Ar initially at atmospheric pressure has been shock-compressed to 0.91 Mbar (Fig. 27). At pressures up to 0.4 Mbar (T≈12,000 K), electronic thermal excitations are negligible, and its properties are determined mainly by the closed-shell interatomic repulsions (Ross, 1980). Shock measurements have also been made starting from the solid (Dick et al., 1970) and from the critical point (van Thiel and Alder, 1966). Above 0.4 Mbar, electron thermal excitations from the closed 3p core to the empty 3d band dominate the Hugoniot, which leads to an observed softening, just as in the case of Xe. LMTO band calculations predict that Ar will become metallic at 5 Mbar and V = 4.5 cm^3 $mole^{-1}$ (McMahan, 1984). Shock-compressed Xe behaves similar to Ar, as reviewed here in Section 3.4.

Helium, the simplest of the inert gases, is the second most abundant element in the solar system; therefore its high-pressure properties are of considerable interest in constructing models of the giant planet interiors. Stewart (1956, 1963) has measured the 4 K isotherm to 20 kbar. The isotherm and ultrasonic longitudinal velocity in fluid ^{4}He have been measured from 75 to 300 K and 2 to 20 kbar (Mills et al., 1980). The melting curve P(T) of ^{4}He has been studied to 160 kbar (360 K) (Loubeyre et al., 1984). The solid phase along the melting curve is hcp to 1 kbar and then fcc up to 116.5 kbar (299 K). At this pressure a cusp has been observed which points to the existence of a triple point and a new high-pressure phase in the solid, believed to be bcc. Isobaric molecular dynamics calculations confirm these observations (Levesque et al., 1983).

The He equation of state has been calculated to 250 Mbar at 0 K by the LMTO method (Young et al., 1981). Metallization occurs at extreme compression, when the bottom of the initially empty 2p band drops below the Fermi level. For the bcc, fcc, and hcp structures, metallization is found to occur at pressures of 31.5, 97, and 112 Mbar, respectively, corresponding to volumes of 0.539, 0.310, and 0.291 cm^3/mole. But hcp is the most stable lattice over this pressure range so that the highest figure is likely to be the 0 K metallization pressure. In the past the difficulty of shock experiments with a liquid He sample has prevented studies from being carried out. Recently, Nellis et al. (1984a) have achieved a pressure of 160 kbar (about 12,000 K and three-fold compression) in a single-shock experiment and 560 kbar (about 21,000 K and five-fold compression) using a reflected shock. These results have been used to determine an effective dense helium pair potential. This potential is significantly softer than those obtained from two-body potentials from molecular beam and Hartree-Fock calculations, pointing to the importance of many-body effects at high density.

4.1.2 Molecular Fluids

Molecular fluids introduce two new features: non-sphericity and chemical decomposition. Over most of the conditions attained in liquid shock-compression studies, the temperatures are sufficiently high to consider molecules to be rotating freely and having spherically symmetric potentials. Johnson et al. (1984) demonstrated, with an extensive set of molecular dynamics results for dense liquid N_2 up to 12,000 K, that an effective spherical potential very accurately models the equation of state for the anisotropic potential.

The first shock-wave measurements on liquid hydrogen were carried out by van Thiel and Alder (1966) using high explosives to obtain a reported pressure of 40 kbar. More recent work by van Thiel et al. (1973), Dick and Kerley (1980) and Nellis et al. (1983) and its relationship to the current static work on the solid phase has been reviewed in Section 4.6. One objective of all these studies has been to determine a spherically symmetric, effective potential which can be used to calculate the metallic transition. Silvera and Goldman (1978) made a very careful theoretical study of the D_2 isotherm at 4 K and up to 26 kbar, using self-consistent phonon theory. Subsequent studies (Young and Ross, 1981) showed that Silvera and Goldman's potential would also correctly predict the fluid isotherms of H_2 and D_2 from 75 to

300 K up to 20 kbar and the experimental melting curves to 57 kbar (Liebenberg et al., 1978; Mao and Bell, 1979; Diatschenko and Chu, 1981). However, this data provides no information about the short-range repulsive force that determines the shape of the Hugoniot and the molecular to metallic transition pressure. By modifying the potential at small separations, it is possible to fit the shock data while maintaining the excellent agreement with the lower-pressure fluid, solid, and melting data (Ross et al., 1983). The high temperatures achieved in hydrogen shock experiments up to 7000 K provide information about the pair potential down to molecular separations of about 1.6 Å, or comparable with separations at which the molecular-metallic transition is believed to take place.

A considerable simplification in the choice of potential parameters has emerged from the recognition that for shock-compressed fluids the spherical pair potentials approximately obey the corresponding-states scaling principle (Ross and Ree, 1980). That is, for two fluids the ratios of the depths of their potential wells (ε) are in the same ratio as their critical temperatures (T); and the cubes of their characteristic length scales (r^*) are in proportion to their critical volumes (V_c). As a result of having fitted parameters to the Ar potential, it has been possible to predict within experimental error the Hugoniot curves for most molecular liquids. This means that the repulsive forces which dominate the high-temperature properties have similar functional dependencies for most fluids. An exception is hydrogen, which has a much softer repulsive force than other closed-shell molecules.

Shock-wave data for O_2 and CO_2 to nearly 1 Mbar are unexceptional and in good agreement with theoretical-calculation-based corresponding states scaling of the pair-potential from Ar (Ross and Ree 1980). For O_2 this is somewhat surprising, considering the interesting behavior of the compressed solid. The Raman and optical spectra, and the phase diagram (Nichol and Syassen, 1983; Yen and Nicol, 1983) of solid O_2 has been studied up to 400 kbar near 298 K. Many interesting features appear which are not present in other diatomics, apparently due to the open-shell triplet ground state. Prominent among these is the dramatic change in color which appears above 100 kbar and the anomalously high melting-pressure curve (Nicol et al., 1979). In contrast the data for N_2 (Nellis and Mitchell, 1980) and CO (Nellis et al., 1981) suggests some molecular breakup (Fig. 28). Both molecules have almost the same critical properties and thus the same effective pair-potential and

molecular Hugoniot is predicted. The qualitative differences apparent in the experimental H_2 and CO Hugoniots reflect the fundamental differences in the nature of their final states. For the case of N_2, the divergence between theory and experiment above 300 kbar is possibly due to dissociation and formation of a monatomic metallic-like fluid. Diamond-anvil measurements on solid N_2 to 400 kbar at 300 K show no unusual behavior (LeSar et al., 1979), suggesting that the shock breakup is thermally induced. CO probably decomposes into carbon and CO_2.

Chemical decomposition is known to occur in hydrocarbons. Yakusheva et al. (1971, 1977) have shown that shock compression of many transparent and colorless hydrocarbons above about 100 kbar and 1000 K is accompanied by a break in the Hugoniot curve and a sharp increase in the light absorbance, resulting in a loss of transparency. These features suggest a rapid pyrolysis of the initial molecule and the formation of an opaque carbon condensate (i.e., tars, graphite). Much f the more recent literature is reviewed by Nellis et al. (1984b). Liquid CS_2 exhibits similar behavior when it is shock compressed to approximately 60 kbar (Sheffield and Duvall 1983) and statically compressed to about the same pressure (Bridgman, 1942).

Theoretical calculations of hydrocarbon Hugoniots, including methane, predict that shock heating induces C-H bond scission and favors the condensation of C atoms into elemental carbon. By considering that the hydrocarbons have been converted to a mixture of carbon and H_2, and using the known equations of state of these materials, it is possible to calculate Hugoniots that agree with experiment (Ree, 1979; Nellis et al., 1984b). Sheffield and Duvall made similar calculations for liquid CS_2 in which they assumed the final product is a stoichiometric mixture of carbon and sulfur.

Pucci and March (1981) have proposed a model for the shock-compressed aromatic planar molecules (benzene, anthracene, etc.) in which the delocalized π electrons form localized bonds between different molecules; the shortening of the bond distance leads to the observed density increase. Clearly, any model which invokes a volume collapse is consistent with the observed behavior, but the difficulty comes with attempting to properly account for the chemical thermodynamics in a direct calculation of the Hugoniot.

4.2 Hot Expanded Metals

In contrast to insulating fluids like Ar, metals can transform continuously from a "metallic" to a "non-metallic" state, and rigorous models

do not exist for calculating thermophysical properties. Experimental studies are greatly restricted by the large binding energies and the high values of critical properties. The critical data have been measured for only Hg, Cs, Rb, and K. Critical values for Mo, Pt, Ir and V have been estimated from the results of isobaric experiments, and those for Ni, Al, Cu and Pb from the expansion isentropes of shock-wave studies on the porous metals. Static methods have been employed to study thermophysical, optical and transport properties of Hg, Cs, Rb and K over the liquid-vapor range up to 20 kbar and 2000 K (Hensel, 1981). Whereas dynamic measurements are made in a sufficiently short time to avoid containment problems, static methods are limited by sample reactivity at high temperatures and by vessel strength at high pressures.

The isobaric expansion technique (see for example Gathers, 1983) is capable of producing states up to 8000 K and twofold-expanded in metals at several kilobars of pressure. A wire sample 1-mm in diameter and 25-mm long is electrically heated in a pressure vessel filled with inert gas, while the heating current, sample voltage drop, diameter and surface temperature are continuously recorded. The inert gas prevents contamination of the sample and provides an isobaric environment. The electrical energy input is equal to the enthalpy change. The heating current rises in 5 μs, fast enough to avoid hydrodynamic collapse of the liquid-metal wire but slow enough for the sample to be near thermodynamic equilibrium at all times. The volume change is recorded by shadowgraph methods. Temperature measurements are made with a multi-channel optical pyrometer, while the electrical resistivity is measured simultaneously. Expansion data for metal Al is shown in Fig. 29. Measurements have been made for Ta, Mo, U, Pb, W, V, Ir, Al and Cu.

A second dynamic method is based on the impedance-matching of expansion isentropes of strongly shocked porous metals (Fortov et al., 1974; Al'tshuler et al., 1980) (See Fig. 25). A shock-wave compresses and heats a sample to state A' in Fig. 7 in an experimental setup similar to Fig. 6d. When the shock emerges from the interface, it expands isentropically and generates a shock-wave into a barrier substance (anvil) of very low impedance (well below C). If the Hugoniot curve of the barrier is known, a measurement of the shock velocity is sufficient to determine the pressure (P) and mass velocity (U) by virtue of the impedance matching. By using different barrier materials such as light metals, plastics and compressed gases, it is possible to determine P,

V, E over a wide range of conditions (Fig. 30). Experiments that start by first shocking a porous metal sample achieve higher temperatures and lower densities than those with solid-like density, and consequently undergo much larger expansions. Measurements have been made for porous Ni, Al, Cu and Pb. The data covers a range of about four orders of magnitude in pressure, extending from the dense liquid metal to the metallic vapor, and has been used to obtain estimates of the critical temperature.

Despite the impressive conditions attained by the dynamic methods, static experiments have more available diagnostic techniques, providing the most detailed understanding of expanded metals and the insulator-metal transition. Because of its relatively low critical temperature, Hg yields extensive experimental results, including dc conductivity, thermoelectric power, Hall effect, knight shift and optical absorption (Hensel 1981). All these properties establish the existence of a metal-nonmetal transition in the range between 8 and 11 g/cm^3 (ρ_c = 5.7 g/cm^3) where Hg exhibits a rapid variation in many of its thermodynamic and transport properties (Cusak, 1982). For divalent Hg, the metal-nonmetal transition is possibly related to an overlap of the valence and conduction bands, making Hg an untypical metal. This is supported by the anamolously low V_c/V_0 values for Hg and its markedly different compressibility factor $Z_c = P_cV_c/RT_c = 0.385$ ($Z_c = 0.22$ for Cs and Rb). From recent measurements of the electrical properties of Cs, Rb and K (Hensel, 1981) and Al (Fig. 29), it appears that in the fluid these metals obey nearly free electron behavior over a density range down to about 50% of the normal melting point density (twice the critical density). Hensel (1981) believes "that at present there is no experimental observation which definitely demonstrates a connection between thermodynamic effects and the metal-nonmetal transition."

4.3 Degenerate Plasmas

The classical one-component plasma (OCP) is an idealized system of ions immersed in a uniform neutralizing electron sea. This system is characterized by the Coulomb coupling parameter $\Gamma = (Ze)^2/r_skT$, where r_s is the ion sphere radius = $(3V/4\pi N_i)^{1/3}$, N_i is the number of ions, and V is the volume of the system. The OCP is a reasonable model for the description of super-dense, completely ionized matter typical of extreme astrophysical conditions (e.g., white dwarfs and neutron stars). Under these conditions the

electrons are highly degenerate ($kT \ll E_f$) and play the role of a uniform background fluid. At sufficiently high density, the energy of such a system may be written as

$$E = \frac{3}{2} N_i kT + N_e\left(\frac{3}{5}\epsilon_F + \epsilon_{ex} + \epsilon_{corr}\right) + U \qquad (4.5)$$

where U is the internal energy of the ion-ion Coulomb interaction in the presence of the homogeneous electron fluid. The electron term above includes the kinetic energy 3/5 ϵ_F, exchange energy ϵ_{ex}, and correlation energy ϵ_{corr}. Slattery et al. (1982) have determined the OCP equation of state and melting point to high accuracy using very long Monte Carlo runs. The internal energy and the free energy have been fitted as function of Γ for both the liquid and solid. An interesting feature is that no observable volume change occurs at the melting transition.

However a real plasma is a two-component system. Even a highly degenerate electron gas will be polarized by the ion-electron interaction, consequently screening the ion-ion interaction. Hubbard and Slattery (1971) accounted for this effect through the use of an electron gas dielectric constant in a weak screening approximation. These calculations have been extended to mixtures for the case of fully ionized H and He ions in a weakly screened electron background. The thermodynamic data have been fitted by a convenient analytic function valid for the full range of compositions from pure H to pure He at pressures of astrophysical interest (Hubbard and DeWitt, 1976). These results are of considerable interest with regard to models of the planets Jupiter and Saturn.

These exact data have stimulated a renewed interest in examining integral equation methods, in particular the hypernetted-chain (HNC) equation. A mathematical explanation of the HNC lies beyond the constraints on this review. But a good introduction is to be found in Croxton (1974). The general reader should consider the HNC to be a method by which accurate thermodynamic properties and pair distribution functions may be calculated for given interparticle potentials. It has been found that the HNC equation, and in particular an augmented-HNC which includes the bridge graphs, are very accurate for treating Coulomb systems (Rogers et al., 1983; Lado et al., 1983). Comparisons of these results with the most accurate Monte Carlo energy calculations and pair-distribution functions for the OCP shows a very close

agreement. The augmented-HNC OCP structure factor has been tabulated for $0.1 \leq \Gamma \leq 180$ (Rogers et al., 1983). HNC methods promise to be increasingly useful for dense plasma studies.

4.4 Nonideal Partially Ionized Plasmas

The properties of partially ionized plasmas may be described by several quantities; the Debye length, $r_D = \left(\frac{kT}{4\pi \sum z_i^2 e^2 \rho_i}\right)$, which is a measure of the extent of the screened Coulomb potential, and two dimensionless parameters characterizing the degree of nonideality and quantum degeneracy of the fluid. The nonideality parameter, $\Gamma = \frac{z^2 e^2}{r_D kT}$ is the ratio of Coulomb energy to kinetic energy, and the quantum degeneracy, $\gamma_e = \left(\frac{h^2}{2\pi m\, kT}\right)^{3/2} / r_D$, compares the electron DeBroglie wavelength to the Debye interaction length. In the simplest theory, the Saha model (γ_e and $\Gamma \ll 1$), the ions and classical free electrons are in chemical equilibrium, and nonideality and quantum effects are neglected. The Debye-Hückel approximation (γ_e and $\Gamma < 0.2$) is valid for small nonideality. Recent work in partially ionized plasmas has moved in the direction of strongly coupled systems having characteristic parameters near or above unity.

Fortov and coworkers in the U.S.S.R. (Fortov, 1982; Mintsev and Fortov, 1983; Alekseev et al., 1983) have recently reviewed the properties of nonideal plasmas of Ar and Xe using explosive-driven shock-tubes. Starting with dense Ar and Xe gas at room temperature, pressures up to 39.2 kbar in Xe and 16.3 kbar in Ar may be achieved with densities up to half that of the liquid phase. This large range of conditions covers a broad spectrum of possible plasma conditions up to $\Gamma \sim 3$. Shock compression experiments of Cs vapor have achieved the final conditions: P about 1.4 to 200 bar, T about 600 to 20,000 K, and nonideality parameters Γ about 0.2 to 2.2. Electrical conductivity and opacity measurements have also been reported. Accurate results are difficult to obtain in this regime because the large compressions lead to large uncertainties in the final density and pressure.

Dense plasma properties are generally calculated using the "chemical" and "physical" models. The chemical model is the simpler and more widely used. It is a philosphical descendent of the Saha and Debye models, described in a series of papers by Graboske et al. (1969, 1971). Gryaznov, et al. (1980) have extended the model to higher densities ($\Gamma \sim 3$). Recently, a third approach has been tried, involving the use of electron-ion pseudopotentials.

4.4.1 Chemical Model

The chemical model is intuitively appealing in that it assumes the partition function to be separable into distinct terms which permit the Helmholtz free energy (A) to be written as a sum of contributions:

$$A = A_{trans} + A_{Coul} + A_{HS} + A_{int} . \qquad (4.7)$$

A_{trans} is the translational free energy of ions and electrons. A_{Coul} is the contribution from the Coulomb interaction of all nonbound particles. It includes the "ring" and "ladder" diagrams of many-body theory, and the electron exchange. A_{HS} is a hard-sphere free energy and serves to simulate ion-ion repulsions. A_{int} is the internal partition function of bound electrons in the ion. The electron energy levels are determined by solving the Schrödinger equation in a sphere, outside of which the potential is infinite and the wave function is zero. The sphere may be equal to the average atomic volume or determined by the hard-sphere diameter. Electrons with positive energy are considered free and contribute to translational and Coulomb terms. As a result, discontinuities in the thermodynamic properties arise when energy levels undergo changes of sign and electrons are transferred from internal bound to translational free states. The free energy is determined by minimizing with respect to the composition of chemical species and hard-sphere diameter. Gryaznov et al. (1980) use that value of the hard-sphere diameter as the atom sphere boundary for solving the Schrödinger equation of the bound electrons. In the chemical model all the degrees of freedom are coupled, and thermodynamically self-consistent calculations have been carried out. The major limitation stems from the artificial nature of the separation between bound and free electrons.

4.4.2 Physical Model

These difficulties are avoided by the more rigorous "physical" approach, which represents a consistent quantum statistical-mechanical treatment of the many-body problem that does not make distinctions between bound and free electrons (Eibeling et al., 1977). In practice, the theory is much more complicated than the chemical model, making the construction of a suitable computer program extremely laborious. Calculations for this model have recently been reported by Rogers (1981) in a paper on the equation-of-state of

dense partially degenerate reacting plasmas. The starting point of the theory is an activity expansion of the grand partition function. The leading terms are the Saha ionization equilibrium equation and Debye-Hückel correction. Higher-order terms resemble many-body virial and cluster coefficients for Coulomb potentials. The theory allows for (1) formation of electron-nucleus composites, (2) coupling of heavy ions, and (3) moderate (gas-like) coupling between electrons. To carry out numerical calculations, it is necessary to obtain multi-electron bound and scattering states. This is accomplished through the introduction of effective electron-ion pair potentials. The parameters in the potential are determined from experimental spectroscopic data, and plasma-screening effects are then added to the long-range tail.

4.4.3 Electron-Ion Pseudopotential Model

The properties of nonideal plasmas can be obtained by the use of classical electron-ion pseudopotentials which have quantum effects built-in as a short range repulsion, but which go over to the Coulomb potential at large distances. In the simplest approximation, charges of the same sign interact through the Coulomb potential ($\phi = e^2/r$) and the interaction of electrons and ions is described by the expression

$$\phi_{ei} = \begin{cases} -\epsilon & r \leq a , \\ -e^2/r & r > a , \end{cases} \qquad (4.8)$$

where ϵ and a are constants determined by some convenient argument. The properties for this two-component plasma have been calculated by Monte Carlo methods (Zelener et al., 1974) by summing over all the pair interactions as in a purely classical system. Equation (4.8) is similar to the Heine- Abarenkov potential widely used in solid state physics, in which the constant potential region at small separations describes the orthogonality repulsion between core and conduction electrons. Calculations have also been made using Yukawa-like screened Coulomb potentials (Dunn and Broyles, 1967; Hansen and McDonald, 1978).

A non-empirical temperature-dependent pseudopotential can be determined from the Slater sum by the condition that the probability density of an electron at a distance r from the nucleus must be equal to the pair distribution function:

$$g_{ei}(r,t) = \left[\frac{2\pi\beta h^2}{2\mu_{ei}}\right]^{\frac{3}{2}} \sum_{E_\alpha}^{\infty} |\psi_\alpha(r)|^2 \exp\{-\beta E_\alpha\} = \exp\{-\beta\phi_{ei}(r,T)\} \quad , \quad (4.9)$$

where the sum is over all states of discrete and continuous spectra and ψ_α and E_α are the complete set of orthonomalized wave-functions and eigenvalues. Barker (1971) has given an exact evaluation of the two-particle Slater sum for a hydrogen plasma. At sufficiently low temperatures, where the deep bound states dominate the sum, the short-range part of the effective potential becomes unrealistically deep. At these conditions the deep levels are partially occupied, restricting the actual space available to the more loosely bound electrons. The difficulty can be corrected by separating the Slater sum into bound state and continuum parts, then subtracting the bound state (Larken, 1960, and Zelener et al. 1972). This has the effect of excluding electrons from the core and leads to a more repulsive and realistic potential. Pseudopotentials obtained this way have been used in with HNC equation to obtain the equation of state and pair distribution functions of dense partially ionized plasmas (Rogers, 1984).

Dharma-Wardana and Perrot (1982) have developed a method for solving the density-functional theory for a neutral system of ions and electrons by the HNC method. For a given temperature and free-electron density, the theory self-consistently determines the various pair distribution functions, bound states, and effective ion charge.

5.0 Planetary Interiors

The planets may be organized into two groups -- the inner or terrestrial planets (Earth, Venus, Mars, and Mercury), and the outer or giant planets (Jupiter, Saturn, Uranus and Neptune). Pluto consists mainly of solidified gases and more closely resembles a moon of a giant planet. The terrestrial planets are constructed mainly from metals, silicates and oxides. The giant planets are believed to have inner rock cores, similar in composition to a terrestrial planet, but surrounded by layers of molecular fluids made up of H, He, N, O, and C. The structure of a planet depends on the original composition of its zone of formation, its evolutionary history, and the equation of state of its composition (Zharkov and Trubitsyn, 1978; Cook, 1980).

The simplest model, the static model of planetary structure, assumes that the planet is in hydrostatic equilibrium and that the evolutionary time scale

greatly exceeds response times in the planet's interior. The relationship between pressure, density, and depth is given by Newton's law of gravitation,

$$\frac{dP}{dr} = -\frac{GM(r)\rho(r)}{r^2} \quad (5.1)$$

where M(r) is the mass interior to the planet at a radius r and $\rho(r)$ is the density.

5.1 The Earth's Deep Interior

Our knowledge of the Earth's interior is derived from seismic data which allows a determination of the density versus depth and pressure versus depth (see for example Dziewonski and Boschi, 1980). The seismic data provides a picture of the Earth divided into crust, upper and lower mantle, liquid outer core and solid inner core. The major problem facing geophysicists concerns the determination of the composition and temperature profile with depth, for which equation of state data is essential. Much of what has been deduced about the Earth's composition has been based on comparisons of seismologically derived pressure-density profiles with laboratory shock-compression experiments (McQueen et al., 1964, 1967; Ahrens, 1980). The entire range of pressures existing within the Earth's interior, including the core (about 3.5 Mbar), is accessible to laboratory shock-wave studies. A comparison of shock-wave data for candidate materials with the pressure-density profiles in the Earth serves to provide constraints on possible compositional models (Fig. 31). It is clear that the lower mantle can be described as a mixture of silicates and metal oxides. On the other hand the density profile and magnetic properties of the fluid outer core require a metallic-like phase. Shock experiments have shown that the density profile is consistent with an iron outer-core mixture containing about 11 percent oxygen (Jeanloz and Ahrens, 1980) or 8 to 10 percent sulfur (Ahrens, 1979). The strongest evidence for a predominately iron inner core also results from a comparison of seismic models with shock data for Fe-Ni alloy (McQueen and Marsh, 1966). At present it appears that the inner core, which is not well constrained and has only 5 percent of the mass of the entire core, may be composed of nearly pure Fe, or Fe and Ni (Ahrens, 1980; Stevenson, 1981). The inner-core/outer-core boundary then represents not only a phase transition, but a compositional boundary.

The melting temperature of Fe at the inner-core/outer-core boundary provides an essential constraint to the construction of thermal models of the Earth's interior. Brown and McQueen (1980, 1982) have detected melting in Fe on the Hugoniot at 2.5 ± 0.1 Mbar (Fig. 10). At the inner-core boundary pressure of 3.3 Mbar, the melting point for pure Fe is calculated to be about 6000° C (±500° C). Stevenson (1981) and Young and Grover (1984) have constructed a model that is fitted to the Fe shock data and which predicts a melting temperature near 6000° C. But it is clearly too high for the actual core temperature (~3700° C), which is lowered by alloying.

5.2 Giant Planet Interiors

The recent flights of Pioneer 10 and Voyagers 1 and 2 to Jupiter and Saturn, as well as anticipated Voyager visits to Uranus and Neptune, have stimulated a renewed interest in the structure of these giant planets. To construct accurate structural models, it is necessary to explain their observed luminosities, radii, oblateness, rotation rates, and gravitational moments in terms of equations of state for the postulated constituent materials. Several reviews of giant planet models have recently appeared (Hubbard, 1981; Stevenson, 1982; and Smoluchowski, 1983).

The giant planets are thought to consist of three layers: an outer layer of predominately H_2 and non-metallic He; a middle layer either of metallic H and He for Jupiter and Saturn, or of ammonia, methane, and water (referred to as "ices") for Uranus and Neptune; and a rocky core of iron, nickel, silicon, and magnesium oxides. The hydrogen and helium in Jupiter are subjected to a range of conditions from 1 bar and 160 K to 45 Mbar and 24,000 K. In the case of Saturn, which is smaller, the latter two values are roughly 10 Mbar and 10,000 K. The ices in Uranus and Neptune are subjected to pressures between 0.2 and 0.7 Mbar. The rocky core components are compressed to roughly 10 Mbar in Uranus and Neptune and as high as 100 Mbar at Jupiter's center.

Equation of state data relevant to giant planet modeling have been obtained from shock-wave experiments. A comparison of these results for H_2 with the calculated isentropes for Jupiter and Saturn (Fig. 32a) and for the ices (H_2O, NH_3 and CH_4) which form the middle layer of Uranus and Neptune (Fig. 32b) shows that the shock-wave data closely follows the paths of the planetary isentropes. As we have seen, shock-wave experiments on "ice" liquids indicate that over the range of the H_2O and NH_3 are almost totally

ionized and the CH_4 has been pyrolyzed to C and H. Thus a proper model of Uranus and Neptune must correctly account for the thermal chemistry of such a mixture.

Jupiter is the best understood of the giant planets. As noted by DeMarcus (1958), the general structure of the planet is determined primarily by the equation of state of hydrogen. Although Saturn is considered to have a composition similar to Jupiter, until recently no models of that planet were believed to be consistent with all the observables. From the point of view of theoretical modeling and equation of state studies, Saturn has been the most interesting of the major planets. The principal barrier to understanding this planet has stemmed from the apparent failure of evolutionary models to explain the intrinsic heat flow which had been calculated to be two to three times smaller than observed (Graboske et al., 1975; Pollack et al., 1978; Grossman et al., 1980). Evidently Saturn appeared to be emitting more energy than could be explained by the loss of primordial heat. To explain this, Stevenson and Salpeter (1976) proposed a phase separation in the He/metallic-H layer in which the downward migration of the heavier He releases gravitational energy. At a given pressure Saturn has a lower temperature than Jupiter, and if the critical temperature of the mixture were intermediate, then precipitation of He droplets would occur only on Saturn. This spawned a number of theoretical studies for the solubility of fully pressure-ionized H-He mixtures that confirmed in general the existence of a miscibility gap in this system. A serious objection is that He may not be pressure-ionized below 35 Mbar (Young et al., 1981). The highest pressure to which He is subjected to in Saturn is only about 10 Mbar. However the importance of unmixing has faded in the light of recent measurements from the Voyager 1 spacecraft (Hanel et al., 1983), resulting in a considerable downward revision of the heat-flow so that "even homogeneous models which account for the heat flow by a simple cooling mechanism now seem marginally viable" (Hubbard and Stevenson, 1984).

One compelling feature that has followed from the use of improved equations of state based on shock data is a simplification in the planetary models. Earlier giant planet models, using less accurate equations of state, required assumptions of non-solar compositions of the fluid components, with excess He, or excess H_2O or other ices to give structural models that match observations. The molecular-metallic transition of hydrogen is of continued interest. The current estimates of 2 to 4 Mbar are consistent with existing

models but more attention is being paid to the nature of the transition. A first order change would demand a discontinuity in the distribution of compounds and the sharp delineation of layers.

KJA

REFERENCES

Ahrens, T.J., 1979, J. Geophys. Res. 84, 985.

Ahrens, T.J., 1980, Science 207, 1035-1041.

Ahrens, T.J., Lyzenga, G.A., and Mitchell, A.C., 1981, High Pressure Research in Geophysics, Eds. S. Akimoto and M.H. Manghnani (Tokyo: Academic Press) 579-594.

Aidun, J., Bukowinski, M.S.T., and Ross, M., 1984, Phys. Rev. B29, 2611-2621.

Al'tshuler, L.V. and Bakanova, A.A., 1969, Sov. Phys. Uspekhi 11, 678-89.

Al'tshuler, L.V., 1965, Sov. Phys. Usp. 8, 52-91.

Al'tshuler, L.V., Bakanova, A.A. and Dudoladev, I.P., 1968a, Sov. Phys. JETP 26, 1115-20.

Al'tshuler, L.V., Bakanova, A.A., Dudoladov, I.P., Dynin, E.A., Trunin, R.F. and Chekin, B.A., 1981a, J. Appl. Mech. Tech. Phys. 22, 145-169.

Al'tshuler, L.V., Bushman, A.V., Zhernokletov, M.V., Zubarev, V.N., Leont'ev A.A., and Fortov, V.E., 1980, Sov. Phys. JETP 51, 373-83.

Al'tshuler, L.V., Egorov, N., Tochkina, E.V. and Orekin, Yu.K., 1981b, Sov. Phys. JETP. 54, 359-361.

Al'tshuler, L.V., Kalitkin, N.N., Kuz'mina, L.V., and Chekin, B.S., 1977, Sov. Phys. JETP 45, 167-171.

Al'tshuler, L.V., Moiseev, B.M., Popov, L.V., Simakov, G.V., and Trunin, R.T., Sov. Phys. JETP 27, 420-2 1968b.

Al'tshuler, L.V., Voropinov, A.I., Gandel'man, G.M., Dmitriyev, N.A.,and Podval'nyy, 1981c, Phys. Met. Metall. 51, 61-66.

Alekseev, V.A., Fortov, V.E., and Yakubov, I.T., 1983, Sov. Phys. Usp. 26, 99-115.

Anisichkin, V.F., 1978, J. Appl. Mech. Tech. Phys. 19, 376-9.

Asaumi, K., 1984, Phys. Rev. B29, 1118-1120.

Asaumi, K., Mori, T., and Kondo, Y., 1982, Phys. Rev. Lett. 49, 827-40.

Asaumi, K., Susuki, T. and Mori, T., 1983, Phys. Rev. B28, 3529-33.

Asay, J.R. and Hayes, D.B., 1975, J. Appl. Phys. 46, 4789-4800.

Ashcroft, N.W. and Stroud, D., 1978, Solid State Phys. 33 1-81.

Ashcroft, N.W., 1968, Phys, Rev. Lett, 21, 1748-9.

Avrorin, E.N., Vodolaga, B.K., Volkov, L.P., Vladimirov, A.S., Simonenko, V.A., and Chernovolyuk, B.T., JETP Lett. 31, 685-7 1980.

Balchan, A.S. and Drickamer, H.G., 1961, J. Chem. Phys. 34, 1948-9.

Barker, A.A., 1971, J. Chem. Phys. 55, 1751-9.

Barker, J.A. and Henderson, D.H., 1976, Revs. Mod. Phys. 48, 587-672.

Barker, L.M. and Scott, D.D., 1984, "Development of a High-Pressure Quasi-Isentropic Plane Wave Generating Capability," Sandia Report SAND84-0432, Sandia National Laboratory, Albuquerque, NM, USA.

Bassett, W.A., 1979, Ann. Rev. Earth Plant Sci. 7, 357-84.

Bean, V.E., Akimoto, S., Bell, P.M., Block, S., Holzapfel, W.B., Jamieson, J.C., Manghnani, M.H., Nicol, M.F., Permarini, G.J., and Stishov, S.M. in High Pressure in Research and Industry (Uppsala; Arkitektkopia) 1982, pp 144-151.

Benedict, U., Peterson, J.R., Haire, R.G., and Dufour, C., 1984, J. Phys. F: Met. Phys. 14, L43-47.

Bennett, B.I., Johnson, J.D., Kerley, G.I. and Rood, G.I., 1978, "Recent Developments in the Sesame Equation of State Library" Los Alamos Scientic Laboratory Report LA-7130.

Binder, K., 1979, "Monte Carlo Methods," (Berlin: Springer-Verlag).

Birch, F., 1952, J. Geophys. Res. 57, 227-86.

Block, S. and Piermarini, G.J., 1976, Phys Today 29, 44-55.

Bloom, G.H. and Keeler, R.N., 1974, J. Appl. Phys. 45, 1200-1207.

Boehler, R. and Ross, M., 1984, Phys. Rev. B29, 3673-3676.

Boyer, L.L., 1981, Phys. Rev. B23, 3673-85.

Bridgman, P.W., 1942, Proc. Am. Acad. Arts Sci. 74, 399.

Bridgman, P.W., 1948, Proc. Am. Acad. Arts Sci. 76, 55.

Bridgman, P.W., 1958, "The Physics of High Pressures," (London: G. Bell and Sons).

Brovman, E.G., Kagan, Yu., and Kholas, A., 1971, Sov. Phys. JETP, 34, 1300-15.

Brovman, E.G., Kagan, Yu., and Kholas, A., 1972, Sov. Phys. JETP, 35, 783-7.

Brown, J.M. and McQueen, R.G., 1980, J Geophys. Res. 7 533-536.

Brown, J.M. and McQueen, R.G., 1982, in "High-Pressure Research in Geophysics," ed. by S. Akimoto, and M.H. Manghnani (Tokyo: Center for Academic Publications) pp 611-623.

Bukowinski, M.S.T., 1984, private communication.

Bushman, A.V. and Fortov, V.E., 1983, Sov. Phys. Uspekhi 26, 465-96.

Carlsson, A.E., and Ashcroft, N.W., 1983, Phys. Rev. Lett. 50, 1305-8.

Carter, W.J., Fritz, J.N., Marsh, S.P., and McQueen, R.G., J. Phys. Chem. Solids., 1975 36, 741-752.

Cook, A.H., 1980, "Interiors of the Planets," (Cambridge: Cambridge Univ. Press).

Cowan, R.D. and Ashkin, J., 1957, Phys. Rev. 105, 144-157.

Croxton, C.A., 1974, "Liquid State Physics," (Cambridge: Cambridge University Press).

Cusak, N.E., 1982, Prog. Theor. Phys. Suppl. 72, 81-99.

Davison, L. and Graham, R.A., 1979, Phys. Reports, 55 255-379.

Demarcus, W.C., 1958, Astron. J. 63, 2-28.

Dharma-Wardana, M.W.C. and Perrot, F., 1982, Phys. Rev. A26, 2096-104.

Diatchenko, V. and Chu, C.W., 1981, Science, 212, 1393-4.

Dick, R.D. and Kerley, G.I., 1980, J. Chem. Phys. 73, 5264-71.

Dick, R.D., Warner, R.H. and Skalyo, Jr., 1970, J. Chem. Phys. 53, 1648-51.

Drickamer, H.G. and Frank, C.W., "Electronic Transitions and the High Pressure Chemistry of Solids," (London: Chapman and Hall, 1973).

Driessen, A., and Silvera, I.F., 1984, J. Low Temp. Phys. 54, 361-395.

Dugdale, J.S. and McDonald, D., 1953, Phys. Rev. 89 832-4.

Dunn, T. and Broyles, A.A., 1967, Phys. Rev. 157, 156-66.

Duthie, J.C. and Pettifor, D.G., 1977, Phys. Rev. Lett. 38, 564-7.

Duvall, G.E. and Fowles G.R., 1963 in High Pressure Physics and Chemistry, Volume 2, Ed. R.S. Bradley (New York: Academic Press) pp 209-291.

Dziewonski, A.M., and Boschi, E., 1980, "Physics of the Earth's Interior" (Amsterdam: North Holland).

Eibeling, W., Kraeft, W.D. and Kremp, D., 1977, "Theory of Bound States and Ionization Equilibrium in Plasmas and Solids" (Berlin: Akademic-Verlag).

Feynman, R.P. Metropolis, N. and Teller, E., 1949, Phys. Rev. 99 1854-70.

Fortov, V.E., 1982, Sov. Phys. Usp. 25, 781-809.

Fortov, V.E., Leontov, A.A., Dremin, A.N. and Pershin, S.V., 1974, JETP Lett. 20, 13-14.

Fowles, G.R., Duvall, G.E., Asay, J., Bellamy, P., Feistmann, F., Grady, D., Michaels, T., and Mitchell, R., 1970, Rev. Sci. Instrum. 41, 984-96.

Friedli, C. and Ashcroft, N.W., 1977, Phys. Rev. B16, 662-72.

Froyen, S. and Cohen, M.L., 1983, Phys. Rev. B28, 3258-65.

Froyen, S. and Cohen, M.L., 1984, Phys. Rev. B29, 3770-2.

Gandelman, G.M., Ermachenko, V.M. and Zeldovich, Ya.B., 1963, JETP 44, 386-387.

Gathers, G.R., 1983, Int. J. Therms. Phys. 4, 209-26.

Gathers, G.R. and Ross, M., 1984, J. Non-Crys. Sol. 61, 59-64.

Gatilov, L.A. and Kuleshova, L.V., 1981, Sov. Phys. Solid State 23, 1663-5.

Glötzel, D. and McMahan, A.K., 1979, Phys. Rev. B20, 3210-16.

Godwal, B.K., Sikka, S.K. and Chidambaram, R., 1981, Phys. Rev. Lett., 47, 1144-47.

Godwal, B.K., Sikka, S.K. and Chidambaram, R., 1983, Phys. Recpts., 102, 122-197.

Goetell, K.A., Mao, H.K., and Bell, P.M., 1984, EOS Trans. A.G.U. 65, 283.

Graboske, H.C., Harwood, D.J. and Rogers, F.J., 1969, Phys. Rev. 186, 210-25.

Graboske, H.C., Harwood, D.J. and DeWitt, H.E., 1971, Phys. Rev. A3, 1419-31.

Graboske, H.C., Pollack, J.B., Grossman, A.S. and Olness, R.J., 1975, Astrophys. J. 199, 265-281.

Graham, R.A. and Asay, J.R., 1978, High Temp.-High Press. 10 355-390.

Grigorev, F.V., Kormer, S.B., Mikhailova, O.L., Tolochko, A.P. and Urhin, V.D., 1978, Sov. Phys. JETP 48, 847-852.

Grigorev, F.V., Kormer, S.B., Mikhailova, O.L., Tolochko, A.P. and Urhin, V.D., 1972, Sov. Phys. JETP Lett 16, 201-5.

Grossman, A.S., Pollack, J.B., Reynolds, R.T., Summers, A.L. and Graboske, H.C. , 1980, Icarus 42, 358-379.

Gryaznov, V.K., Zhernokletov, M.V., Zubarev, V.N., Iosilevskii, I.L. and Fortov, V.E., 1980, Sov. Phys. JETP, 51, 288-95.

Grzybowski, T.A. and Ruoff, A.L., 1984, submitted to Phys. Rev. Lett.

Gust, W.H. and Royce, E.B., 1973, Phys. Rev B8, 3595-609.

Hamann, S.D., and Linton, M., 1969, Trans. Faraday Soc. 65, 2186-96.

Hanel, R.A., Conrath, B.J., Kunde, V.G., Pearl, J.C. and Pirraglia, J.A., 1983, Icarus, in press.

Hansen, J.P. and McDonald, I.R., 1978, Phys. Rev. Lett, 41, 1379-82.

Hawke, P.S., Burgess, T.J., Durre, D.E., Huebel, J.G., Keeler, R.N., Klapper, H. and Wallace, W.C., 1978, Phys. Rev. Lett 41, 994-7.

Hedin, L. and Lundquist, S., 1971, J. Phys. C4, 2064-83.

Hensel, F., 1981, in "Proceedings of the Eighth Symposium on Thermophysical Properties" ed. J.V. Sengers, p 151-158.

Herzfeld, K.F., 1927, Phys. Rev. 29, 701-5.

Hohenberg, P. and Kohn, W., 1964, Phys. Rev. 136, 864-871.

Holmes, N.C., Mitchell, A.C., Nellis, J.W., Graham, W.B. and Walrafen, G.E., 1983, Lawrence Livermore National Laboratory Report, UCRL-89753.

Homan, C., MacCrone, R. and Whalley, E., 1984, "High Pressure in Science and Technology" (New York: Elvesier).

Hubbard, W.B. and DeWitt, H.E., 1976, Ap. J. 205, 295-301.

Hubbard, W.B. and Slattery, W.L., 1971, Ap. J. 168, 131-9.

Hubbard, W.B. and Stevenson, D.J., 1984, in "Saturn" ed. T. Gehrels (Tucson: University of Arizona Press) in press.

Hubbard, W.B., 1981, Science 214, 145-9.

Iosilevskii, I.L. and Gryaznov, V.K., 1981, High Temperature, 19, 799-803.

Jayaraman, A., 1983, Rev. Mod. Phys. 55, 65-108.

Jayaraman, A., 1984, Scientific American 250, 54-62.

Jayaraman, A., Newton, R.C. and McDonough, J.M., 1967, Phys. Rev. 159, 527-533.

Jeanloz, R. and Ahrens, T.J., 1980, Geophys. J.R. Astr. Soc., 62, 505-528.

Jeanloz, R., 1981, in "Proceedings of Am. Chem. Soc. 17th State-of-the-Art Symposium."(ACS: Washington DC) pp. 70-76.

Johannson, B., 1974, Phil. Mag. 30, 469-82.

Johannson, B., 1977, J. Phys. F: Metal Phys. 7, 877-83.

Johannson, B., Skriver, H.L. and Anderson, O.K., 1981, in "Physics of Solids Under High Pressure," edited by J.S. Schilling and R.N. Shelton (Amsterdam: North Holland.

Johnson, J.D., Shaw, M.S., and Holian, B.L., 1984, J. Chem. Phys. 80, 1279-1294.

Johnson, Q. and Mitchell, A.C., 1980, in High Pressure Science and Technology, Eds. B. Vodar and Ph. Marteau (Oxford; Pergamon Press) pp 977-978.

Johnson, Q., Mitchell, A.C., and Smith, I.D., 1980, Rev. Sci. Instrum. 51, 741-749.

Jones, A.H., Isbell, W.M., and Maiden, C.J., 1966, J. Appl. Phys. 37, 3493-99.

Kalitkin, N.N. and Kuz'mina, L.V., 1972, Sov. Phys. Solid State, 13, 1938.

Kalitkin, N.N., 1960, Sov. Phys. JETP 11 1106-10.

Kerley, G.I., 1980a, J. Chem. Phys 73, 469-77.

Kerley, G.I., 1980b, Ibid., 478-86.

Kerley, G.I., 1980c, Ibid., 487-94.

Kerley, G.I., 1981, "User's Manual for PANDA: A Computer Code for Calculating Equation of State" Los Alamos National Laboratory Report LA-8833-M.

Kerley, G.I., 1983 in "Molecular Based Study of Fluids" eds. J.M. Hale and G.A. Mansoori (Washington, D.C.: American Chemical Society).

Kim, S.Y. and Gordon, R.G., 1974, 60, 1842-50.

Kirzhnitz, D.A. and Shpatakovskaya, G.V., 1972, Sov. Phys. JETP 35 1088-94.

Kirzhnitz, D.A., Lozovik, E. Yu. and Shpatakovskaya, G.V., 1976, Sov. Phys. Usp. 18, 649-672.

Knittle, E. and Jeanloz, R., 1984, Science 223, 53-56.

Koelling, D.D., 1981 Rep. Prog. Phys. 44, 139-212.

Kormer, S.B., 1968, Sov. Phys.-Uspeki, 11, 229-254.

Kormer, S.B., Funtikov, A.I., Urlin, V.D., and Kolesnikov, A.N., 1962, Sov. Phys. JETP, 15, 477-488.

Kormer, S.B., Sinitsyn, M.V. and Kuryapin, A.I., 1969, Sov. Phys. JETP, 28, 852-854.

Kovel, M.I., 1973, "The Shock Wave Hugoniot and Electrical Conductivity of Liquid Ammonia in the Pressure Range 45 kbar to 282 kbar," Lawrence Livermore National Laboratory Report-UCRL 51367.

Krupnikov, K.K., Brazhnik, M.I. and Krupnikova, V.P., 1962, Sov. Phys. JETP 15, 470-476.

Lado, F., Foiles, S.M. and Ashcroft, N.W., 1983, Phys. Rev. A28, 2374-9.

Lam, P.K. and Cohen, M.L., 1981, Phys. Rev. B24, 4224-9.

Lam, P.K., Chou, M.Y. and Cohen, M.L., 1983, Phys. Rev. 28B, 4179-85.

Larken, A.I., 1960, JETP, 11, 1363-4.

Latter, R., 1955, Phys. Rev. 99, 1854-1870.

Latter, R., 1956, J. Chem. Phys. 24, 280-292.

LeSar, R. and Gordon, R.G., 1982, J. Chem. Phys. 77, 3682-92.

LeSar, R. and Gordon, R.G., 1983, J. Chem. Phys. 78, 4991-6.

LeSar, R., Ekberg, S.A., Jones, L.H., Mills, R.L., Schwalke, L.A., and Shiferl, D., 1979, Sol. State Comm. 32, 131-4.

Levesque, D., Weis, J.J., and Klein, M.L., 1983, Phys. Rev. Lett. 51, 670-3.

Liberman, D.A., 1976, Int. J. Quant. Chem. Symp. 10, 297-03.

Liberman, D.A., 1979, Phys. Rev. B20, 4981-89.

Liebenberg, D.H., Mills, R.H. and Bronson, J.C., 1978, Phys. Rev. B18, 4526-32.

Loubeyre, P., Besson, J.M., Dinceaux, J.P. and Hansen, J.P., 1982, Phys. Rev. Lett. 49, 1172-5.

Lunqvist, S. and March, N.H., 1983, "Theory of Inhomogeneous Electron Gas," (New York: Plenum Press).

Lyzenga, G.A. Ahrens, T.J., Nellis, W.J., and Mitchell, A.C., 1982, J. Chem. Phys. 76, 6282-6286.

Lyzenga, G.A. and Ahrens, T.J., 1979, Rev. Sci. Instrum. 50, 1421-1424.

MacKintosh, A.R. and Anderson, O.K., 1980, in Electrons at the Fermi Surface, edited by M. Springford (Cambridge: Cambridge University Press).

Makarenko, I.N., Goncharov, A.F., and Stishov, S.M., 1984, Phys. Rev. B29, 6018-9.

Mansoori, G.A. and Canfield, F.B., 1969, J. Chem. Phys. 51, 4958-4967.

Mao, H.K. and Bell, P.M., 1979, Science 203, 1004-6.

Mao, H.K., Bell, P.M., Shaner, J.W., and Steinberg, D.J., 1978, J. Appl. Phys. 49, 3276-83.

Mao, H.K., Hazen, R.M., Bell, P.M., and Wittig, J., 1981, J. Appl. Phys. 52, 4572-74.

March, N.H., 1957, Advances in Physics, 21 1-101.

Margenau, H. and Kestner, N.R., 1971, "Theory of Intermolecular Forces" (Oxford: Pergamon Press).

Marsh, S.P., 1980, LASL Shock Data, (Berkeley: University of California Press).

McMahan, A.K. and Albers, R.C., 1982, Phys. Rev. Lett 49, 1198-1201.

McMahan, A.K. and Ross, M., 1979, in High-Pressure Science and Technology, Eds. K.D. Timmerhaus and M.S. Barber (New York: Plenum) 920-926.

McMahan, A.K. and Ross, M., 1977, Phys. Rev. B15, 718-724.

McMahan, A.K., 1984, private communication.

McMahan, A.K., Hord, B.L. and Ross, M., 1977, Phys. Rev. B15, 726-37.

McMahan, A.K., Yin, M.T., and Cohen, M.L., 1981, Phys. Rev. B24, 7210-16.

McQueen, R.G., Marsh, S.P. and Fritz, J.N., 1967, J. Geophys. Res. 72, 4999-5036.

McQueen, R.G., Marsh, S.P. and Fritz, J.N., 1964, J. Geophys. Res. 69, 2947-2965.

McQueen, R.G., and Marsh, S.P., 1966, J. Geophys. Res. 71, 1751-56.

McWhan, D.B., Parisot, G., and Block, D., 1974, J. Phys. F4, L69-75.

Mills, R.L., Liebenberg, D.H., and Bronson, J.C., 1980, Phys. Rev. B21, 5137-48.

Mintsev, V.B. and Fortov, V.E., 1983, High Temperature 21, 623-645.

Mitchell, A.C. and Nellis, W.J., 1981, Rev. Sci. Instrum. 52 347-358.

Mitchell, A.C. and Nellis, W.J., 1982, J. Chem. Phys. 76, 6273-81.

More, R.M., 1979, Phys. Rev. A19, 1234-46.

Moruzzi, V.L., Janak, J.F. and Williams A.R., 1978, "Calculated Electronic Properties of Metals" (Oxford: Pergamon).

Nellis, W.J. and Mitchell, A.C., 1980, J. Chem. Phys. 73, 6137-45.

Nellis, W.J., 1983 in "High Pressure Measurement Techniques" ED. G.N. Peggs (London: Applied Science Publishers).

Nellis, W.J., 1984, private communication.

Nellis, W.J., Mitchell, A.C., Van Thiel, M., Devine, G.J. and Trainor, R.J., 1983, J. Chem. Phys. 79, 1480-86.

Nellis, W.J., Ree, F.H. Van Thiel, M. and Mitchell, A.C., 1981, J. Chem. Phys. 75, 3055-3063.

Nellis, W.J., Mitchell, A.C., Holmes, N.C., Trainor, R.J., Governo, G.K., Ross, M., and Young, D.A., 1984a, submitted to Phys. Rev. Lett.

Nellis, W.J., Ree, F.H., Trainor, R.J., Mitchell, A.C., and Boslough, M.B., 1984b, J. Chem. Phys. 80, 2789-2799.

Nellis, W.J., Van Thiel, M. and Mitchell, A.C., 1982, Phys. Rev. Lett. 816-18.

Nichol, M. and Syassen, K., 1983, Phys. Rev. B28, 1201-1206.

Nicol, M., Hirsch, K.R. and Holzapfel, W.B., 1979, Chem. Phys. Lett. 68, 49-52.

Olinyk, H. and Holzapfel, W.B., 1984, Phys. Lett. 100A, 191-194.

Perrot, F., 1979, Phys. Rev. A20, 586-594.

Pettifor, D.G., 1970, J. Phys. C: Solid St. 3, 367-77.

Pettifor, D.G., 1977, J. Phys. F Metal Phys., 7, 613-33.

Pickett, W.E., Freeman, A.J. and Koelling, D.D., 1981, Phys. Rev. B23, 1266-1291.

Podurets, M.A., Simakov, G.V., Trunin, R.F., Popov, L.V., Moiseev, B.N., Sov. Phys. JETP 35, 375-6 1972.

Pollack, J., Grossman, A.S., Moore, R. and Graboske, H.C., 1978, Icarus 30, 111-128.

Pucci, R. and March, N.H., 1981, J. Chem. Phys. 74, 1373-78.

Radousky, H.B., Ross, M., Mitchell, A.C. and Nellis, W.J., 1984, submitted to Phys. Rev. B.

Ragan III, C.E., 1982, Phys. Rev. A25, 3360-3375.

Ragan III, C.E., 1984, Phys. Rev. A.

Ragan III, C.E., 1980, Phys. Rev. A21, 458-463.

Ragan III, C.E., Silbert, M.G., and Diven, B.C., 1977, J. Appl. Phys. 48, 2860-70.

Raich, J.C. and Etters, R.D., 1972, J. Low Temp. Phys. 6, 229-40.

Ray, A.K., Trickey, S.B., Weidman, R.S. and Kunz, A.B., 1980, Phys. Rev. Lett. 45, 933-5.

Ree, F.H. and Bender, C.F., 1979, J. Chem. Phys. 71, 5363-75.

Ree, F.H. and Winter, N.W., 1980, J. Chem. Phys. 73, 322-36.

Ree, F.H., 1979, J. Chem. Phys. 70, 974-83.

Rice, M.H., McQueen, R.G. and Walsh, J.M., 1958 in Solid State Physics Volume VI, Eds. F. Seitz and D. Turnball (New York: Academic Press) pp 1-63.

Riggleman, B.M. and Drickamer, H.G., 1963, J. Chem. Phys. 38, 2721-4.

Rogers, F.J., 1981, Phys. Rev. A24, 1531-43.

Rogers, F.J., 1984, Phys. Rev. A29, 868-79.

Rogers, F.J., Young, D.A., DeWitt, H.E. and Ross, M., 1983, Phys. Rev. A28, 2990-2.

Rosenfeld, Y. and Ashcroft, N.W., 1979, Phys. Rev. A20, 1208-35.

Ross, M. and McMahan, A.K., 1980, Phys. Rev. B21, 1658-64.

Ross, M. and McMahan, A.K., 1976, Phys. Rev. B13, 5154-7.

Ross, M. and Ree, F.H., 1980, J. Chem. Phys. 73, 6146-6152.

Ross, M. and Shishkevish, 1977, "Molecular and Metallic Hydrogen," Rept. R-2056-ARPA, Rand Corporation, Santa Monica, CA.

Ross, M. and McMahan, A.K., 1981, in "Physics of Solids under High Pressure" ed. by J.S. Schilling amd R.N. Shelton (Amsterdam: North Holland) 161-168.

Ross, M., 1968, Phys. Rev. 171, 777-84.

Ross, M., 1972, J. Chem. Phys. 56, 4651-4653.

Ross, M., 1979, J. Chem. Phys. 71, 1567-1571.

Ross, M., 1980, J. Chem. Phys. 73, 4445-50.

Ross, M., 1980, Phys. Rev. B21, 3140-51.

Ross, M., Nellis, W.J. and Mitchell, A.C., 1979, Chem. Phys. Lett, 68, 532-5.

Ross, M., Ree, F.H. and Young, D.A., 1983, J. Chem. Phys. 79, 1487-94.

Schmidt, S.C., Moore, D.S., Schiferl, D. and Shaner, J.W., 1983, Phys. Rev. Lett., 50, 661-664.

Shaner, J.W. Brown, J.M., and McQueen, R.G., 1984, to be published in "High Pressure Science and Technology" ed by C. Homan, R. MacCrone and F. Whalley, (New York: Elvesier).

Sharma, S.K., Mao, H.K. and Bell, P.M., 1980, Phys. Rev. Lett. 44, 886-8.

Sheffield, S.A. and Duvall, G.E., 1983, J. Chem. Phys. 79, 1981-80.

Shimizu, H., Brody, E.M., Mao, H.K., and Bell, P.M., 1981, Phys. Rev. Lett, 47, 128-131.

Silvera, I.F. and Goldman, V.V., 1978, J. Chem. Phys. 69, 4209-13.

Silvera, I.F. and Wijngarden, R.J., 1981, Phys. Rev. Lett. 47, 39-42.

Silvera, I.F., 1980, Rev. Mod. Phys. 52, 393-452.

Skriver, H.L., 1982, Phys. Rev. Lett. 49, 1768-72.

Skriver, H.L., 1984, "The LMTO Method" (New York: Springer-Verlag).

Skriver, H.L., Anderson, O.K. and Johannson, B., 1980, Phys. Rev. Lett. 44, 1230-33.

Slater, J.C., 1939, Introduction to Chemical Physics (New York: McGraw-Hill).

Slater, J.C., 1951, Phys. Rev. 81, 385-390.

Slater, J.C., 1965, Quantum Theory Molecules and Solids, Vol. 2 (New York: McGraw Hill).

Slater, J.C., 1979, "The Calculation of Molecular Orbitals" (New York: John Wiley and Sons).

Slattery, W.L., Doolen, G.D. and DeWitt, H.E., 1982, Phys. Rev. A26, 2255-8.

Smith, G.S. and Akella, J., 1982, J. Appl. Phys. 52, 9212-3.

Smoluchowski, R., 1983, The Moon and the Planets 28, 137-54.

Sternheimer, R., 1950, Phys. Rev. 78, 235-43.

Stevenson, D.J. and Salpeter, E.E., 1976, in "Jupiter," ed. T. Gehrels, (Tucson: University of Arizona Press) pp 85-112.

Stevenson, D.J., 1981, Science, 214, 611-619.

Stevenson, D.J., 1982, Ann. Rev. Earth Planet Sci. 10, 257-95.

Stewart, J.W., 1956, J. Chem. Solids, 1, 146-58.

Stewart, J.W., 1963, Phys. Rev. 129, 1950-1.

Straus, D.M. and Ashcroft, N.W., 1977, Phys. Rev. Lett. 38, 415-8.

Styris, D.L., and Duvall, G.E., 1970, High Temp. Pres. 2, 447-499.

Syassen, K. and Reichlin, R., 1984, Private communication.

Syassen, K., 1982, Phys. Rev. B25, 6548-50.

Syassen, K., Takemura, K., Tups, H. and Otto, A., 1981, in "Physics of Solids Under Pressure," edited by J.S. Schilling and R.N. Shelton (North-Holland, Amsterdam), p., 125.

Takemura, K. and Syassen, K., 1983, Phys. Rev. B28, 1193-96.

Takemura, K., Miromura, S. and Shimomura, O. and Fujii, K., 1980, Phys. Rev. Lett. 45, 1881-4.

Torrens, I.M., 1972, "Interatomic Potentials" (New York: Academic Press).

Trunin, R.F., Podurets, M.A., Moiseev, B.N., Simakov, G.V. and Popov, L.V., Sov. Phys. JETP 29, 630-1 1969.

Trunin, R.F., Podurets, M.A., Simakov, G.V., Popov, L.V., and Moiseev, B.N., Sov, Phys. JETP 35, 550-2 1972.

Tups, H., Takemura, K. and Syassen, K., 1983, Phys. Rev. Lett. 24, 1776-79.

Van Straaten, J. Wijngarden, R.J., and Silvera, I.F., 1981, Phys. Rev. Lett. 48, 97-100.

Van Thiel, M. and Alder, B.J., 1966, J. Chem. Phys. 44, 1056-65.

Van Thiel, M., Ross, M., Hord, B.L., Mitchell, A.C., Gust, W.H., D'Addario, M.J., Keeler, R.N. and Boutwell, K., 1973, Phys. Rev. Lett. 31, 979-982.

Van Thiel, M., Shaner, M.J., and Salinas, E., 1977, Lawrence Livermore National Laboratory Report UCRL 50108, Vols. 1-3, Rev. 1.

Vereshchagin, L.F., Yakovlev, E.N., and Timofeev, Yu.A., 1975, JETP. Lett. 21, 85-86.

Volkov, L.P., Voloshin, N.P., Mangasarov, R.A., Simonenko, V.A., Sin'ko, G.V., and Sorokin, V.L., Sov. Phys. JETP, Lett. 31, 513-5 1980.

Von Weizsäcker, C.F., 1935, Z. Phys. 96 431.

Voropinov, A.I., Gandelman, G.M. and Poldval'nyi, 1970, Sov. Phys. Uspekhi, 13, 56-72.

Voskoboinikov, I.M., Gogulya, M.F. and Dolgoborodov, Yu.A., 1979, Sov. Phys.-Dokl. 24, 375-376.

Wigner, E. and Huntington, H.B., 1935, J. Chem. Phys. 3, 764-70.

Wijngarden, R.J., Lagendigk, A.D. and Silvera, I.F., 1982, Phys. Rev. B26, 4957-62.

Wood, D.M., and Ashcroft, N.W., 1982, Phys. Rev. B25, 2532-2544.

Yakusheva, O.B., Yakushev, V.V. and Dremin, A.N., 1971, High Temp.-High Press. 3, 261-266.

Yakusheva, O.B., Yakushev, V.V. and Dremin, A.N., 1977, Russ. J. Phys. Chem. 51, 973-975.

Yen, J. and Nicol, M., 1983, J. Phys. Chem. 87, 4616-8.

Yin, M.T. and Cohen, M.L., 1982a, Phys. Rev. B26, 3259-3273.

Yin, M.T. and Cohen, M.L., 1982b, Phys. Rev. B26, 5668-5687.

Yin, M.T. and Cohen, M.L., 1983 Phys. Rev. Lett. 50, 2006-9.

Young, D.A. and Grover, R., Shock Waves in Condensed Matter (Amsterdam: Holland, 1983).

Young, D.A. and Ross, M., 1984, Phys. Rev. B. 29, 682-91.

Young, D.A. and Ross, M., 1981, J. Chem. Phys. 74, 6950-5.

Young, D.A., McMahan, A.K. and Ross, M., 1981, Phys. Rev. B24, 5119-5127.

Zeldovich, Ya. B. and Raizer, Yu. P., 1966, Physics by Shock Waves and High Temperatures Hydrodynamic Phenomena, Vols. 1-2 (New York:Academic Press).

Zeldovich, Ya.B., Kormer, S.B. and Urlin, V.D., 1969, Sov. Phys. JETP, 28, 855-859.

Zelener, B.V., Norman, G.E. and Filinov, V.S., 1972, High Temperature, 10, 1043-52.

Zelener, B.V., Norman, G.E. and Filinov, V.S., 1974, High Temperature, 12, 235-9.

Zharkov, V.N. and Kalinin, V.A., 1971, "Equations of State for Solids at High Pressure and Temperatures" (New York: Consultants Bureau).

Zharkov, Z.N. and Trubitsyn, V.P., 1978, "Physics of Planetary Interiors," ed. W.B. Hubbard, (Tusconi: Pachart Publishing House).

Zubarev, V.N. and Vashchenko, V. Ya., 1963, Soviet Phys. Solid State 5, 653-5.

FIGURE CAPTIONS

Fig. 1. Schematic layout of a diamond-anvil cell. The high strength and available optical path permit pressure measurements to nearly one Mbar.

Fig. 2. Schematic of a shock wave traveling at a velocity U_s driven by a piston moving with velocity U_p.

Fig. 3. Experimental Hugoniots for metals.

Fig. 4. Schematic diagram of explosive-driven shock-wave experiments. In (a) the metal driver plate is placed in direct contact with the high explosive and the sample. The introduction of a free-run in (b) allows the driver plate to accelerate to much higher velocities (after Graham and Asay, 1978).

Fig. 5. In the operation of the two-stage gas gun, (a) hot gases from a gunpowder detonation drive the piston which compresses hydrogen gas in the pump tube. The high-pressure hydrogen then breaks the rupture valve and (b) accelerates a 20-g metal impactor against a target sample at velocities up to 7 km/s (after Nellis, 1983).

Fig. 6. Schematic of various kinds of impact-shock experiments. (a,b) Plate impact; (c) Single-shock Hugoniot measurement; (d) Double-shock Hugoniot measurement; (e) Shock temperature measurement for a transparent liquid; (f) Sound-speed measurement (after Nellis, 1983).

Fig. 7. Schematic for obtaining the Hugoniot data by the impedance-matching technique: (a) matching by direct impact; (b) matching of reflected or release states.

Fig. 8. Single and double shock (principal and reflected) Hugoniots for (a) liquid deuterium (from Nellis et al., 1983) and (b) aluminum (from Nellis, 1983).

Fig. 9. Hugoniot temperature measurements and estimated melting curve for KCl. Adapted from Kormer (1968).

Fig. 10. Elastic wave velocities as a function of pressure along the Hugoniot of iron. The solid curve is the calculated bulk sound velocity (c_B). From Brown and McQueen, 1980, 1982.

Fig. 11. Measured electrical conductivities of H_2O and NH_3. Data of Hamann & Linton (1969) and Mitchell et al. (1980) for H_2O (Δ) and NH_3 ($\square$). Shown also are temperatures measured for H_2O (Lyzenga & Ahrens 1980) and calculated for NH_3 (Kovel 1973).

Fig. 12. Schematic diagram of the experimental arrangement used to produce a strong planar shock in molybdenum. Light pipes were used to determine the arrival times of the shock at three depths in the molybdenum. The Doppler-shifted neutrons from the Mo were detected at the end of a 20-m-long evacuated line-of-sight (LOS) pipe (from Ragan, 1978).

Fig. 13. Ultra-high-pressure Hugoniot points for aluminum (bars), from nuclear explosive experiments compared with a linear-muffin-tin-orbital (LMTO) calculation of the 0 K isotherm and a liquid perturbation theory calculation of the Hugoniot. The LMTO isotherm was used to fit the parameters of a nearly free electron pseudopotential. A Hugoniot was then calculated with a liquid-metal theory which included thermal electron excitation.

Fig. 14. Atomic volumes vs atomic number at P = 0. Solid curves are experimental values. Dashed curves are for the statistical models. The electron band theory results (o) are mainly the work of Moruzzi et al. (1978) and Skriver (1982).

Fig. 15. a) Comparison of LMTO band theory and TFD 0 K isotherm for lithium as a function of compression V_o/V. b) thermal equation of state of lithium plasma at p = 1 bar in the approximations of Saha (1) TF (2) and TFC (3) (from Iosilevskii and Gryaznov, 1982).

Fig. 16. Schematic energy level diagram as a function of volume. Dashed line represents the Fermi energy of a metal, d_B and d_T are the bottom and top of the d band, and s_B is at the bottom of the s band.

Fig. 17. Cesium 298-K pressure as a function of relative volume. In qualitative agreement with experiment, the theoretical T = 298 K calculation (solid curve) shows an isostructural transition, i.e. the van der Waals loop. The difference between the solid curve and the T = 0 K static lattice pressure $P_o(V)$ (dashed curve) is $3NkT\gamma/V$.

Fig. 18. Shock-pressure vs volume for liquid Xe. The initial volume (V_o) is 44.4 cm^3/mole. Theoretical curves A and B include electronic excitation. Curve C is the pure insulator case (from Nellis et al., 1982).

Fig. 19. Hugoniot curves of alkaline (a) and transition (b) metals (after Al'tshuler et al., 1968). Note the shifted compression scale.

Fig. 20. (a,b) Hugoniots of rare earth elements (after Al'tshuler et al., 1968). Note the shifted compression scale.

Fig. 21. Elements arranged according to the slopes of the U_s-U_p curves (after Al'tshuler et al., 1981).

Fig. 22. The systematic variation of the band gap in the isoelectronic series Xe, CsI, BaTe plotted against the natural logarithm of the specific volume, normalized by the metallization volume (V_H), as predicted by the Herzfeld theory. (after Aidun et al., 1984.)

Fig. 23. Experimental (dots and bars) and theoretical (solid curve) iodine Hugoniots. The completed Hugoniots in the range 0.5 to 3.0 Mbar show the gradual transition from the molecular to the monatomic phase. Softening of the monatomic Hugoniot at higher pressure appears due to thermal electron excitation from the 5p core to 5d conduction states.

Fig. 24. Solid hydrogen isotherms. The solid curve (theory) was calculated using the intermolecular potential obtained from the shock data in Fig. 8. The circles are experimental values.

Fig. 25. Schematic of the phase diagram (dotted lines) with several of the experimental trajectories of particular interest to this review.

Fig. 26. Many-body effects in H_2-H_2 potential. Comparison of the hydrogen pair potential obtained from *ab initio* H_2-H_2 calculations with one obtained from shock data.

Fig. 27. Liquid Ar Hugoniot. Experimental results of Nellis and Mitchell (1980) are shown with error bars. Theoretical curve labeled INS was computed using an intermolecular potential and does not include electronic excitations. The curves labeled WS and APW refer to Hugoniots calculated using conduction-band gaps predicted by the Wigner-Seitz and augmented plane wave methods. (Ross, 1980).

Fig. 28. Single-shock compression curves (Hugoniots) for liquid N_2 (Nellis et al., 1984) and CO (Nellis et al., 1981) The dash-dot curve is obtained from corresponding states theory, neglecting dissociation. Both molecules have almost the same critical properties, thus corresponding-states theory should predict the same molecular Hugoniot.

Fig. 29. Thermal expansion (a) and electrical conductivity; (b) of isobarically ($\sim$ 3kbar) expanded liquid aluminum. The normal solid volume is 10 cm^3/mol. The error bars correspond to $\pm$ 6%. Solid lines are theoretical calculations made from nearly-free electron theory and a local electron-ion pseudopotential model. (Gathers and Ross, 1984).

Fig. 30. Phase diagram of lead. Porous shock adiabat, m (degree of porosity) = 1.25; S is the expansion isentrope; point cr is the estimate of the critical point (after Fortov et al., 1974).

Fig. 31. Shock-wave equations of state (Hugoniots) of simple-oxide and Fe phases compared with the seismologically determined pressure-density profiles of the Earth's lower mantle and outer core. The dashed sections indicate regions of anomalous compression believed to correspond to phase transformations occurring under shock-loading. (from Jeanloz, 1981.)

Fig. 32. (a) Comparison of experimental shock-wave results with the isentropes for Jupiter and Saturn. (b) Plot of experimental shock-wave data for water, ammonia, and methane in the range of temperatures and pressures predicted in the Uranus (and Neptune) "ice" layer.

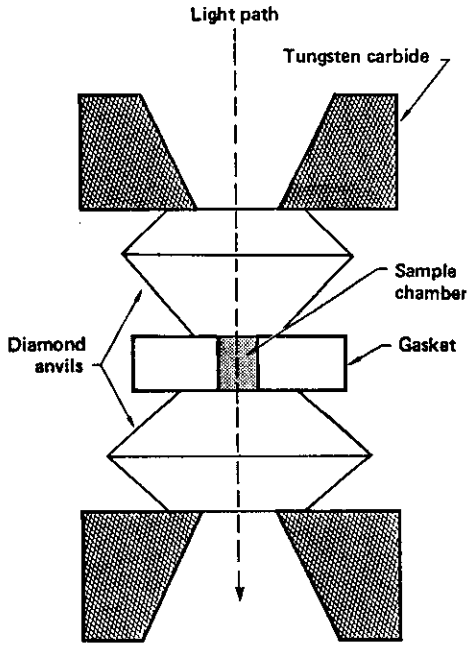

Ross -- Fig. 1

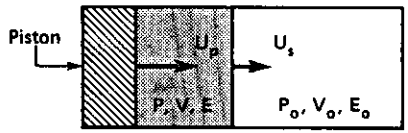

Ross -- Fig. 2

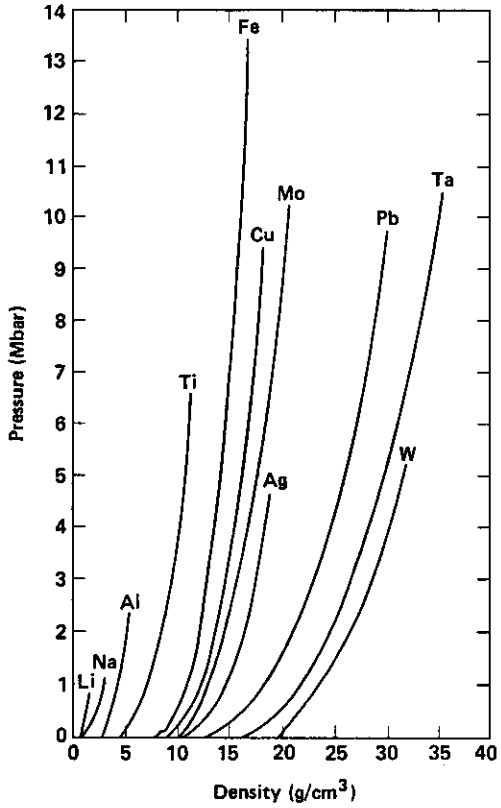

Ross -- Fig. 3

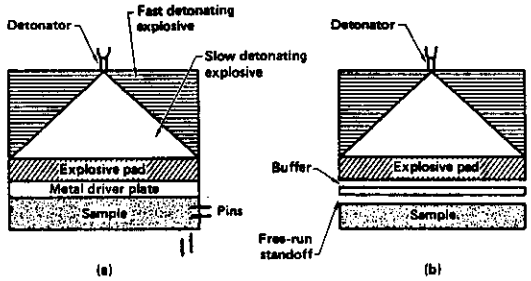

Ross -- Fig. 4

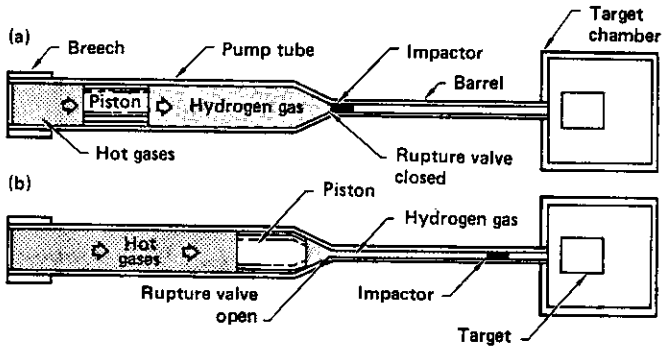

Ross -- Fig. 5

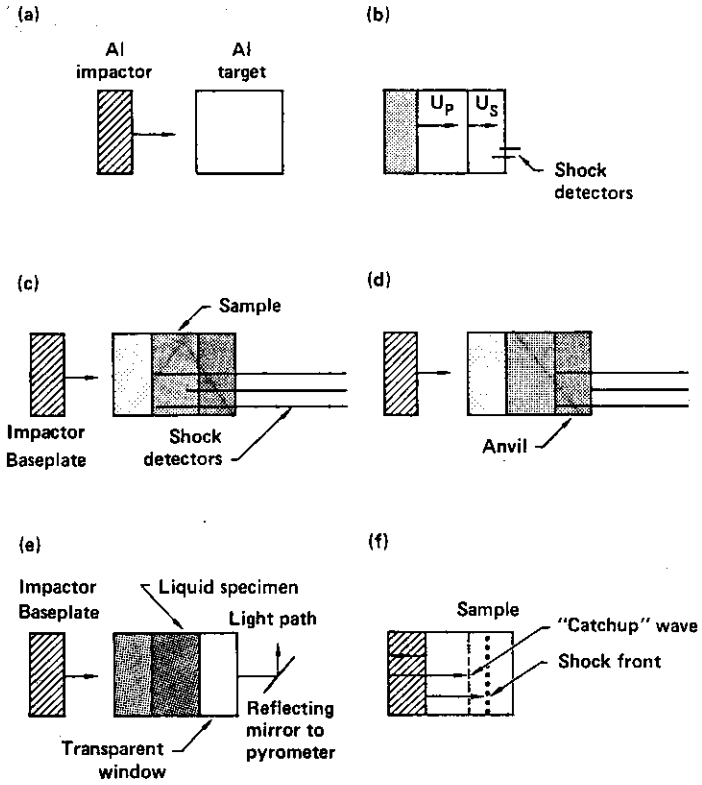

Ross -- Fig. 6

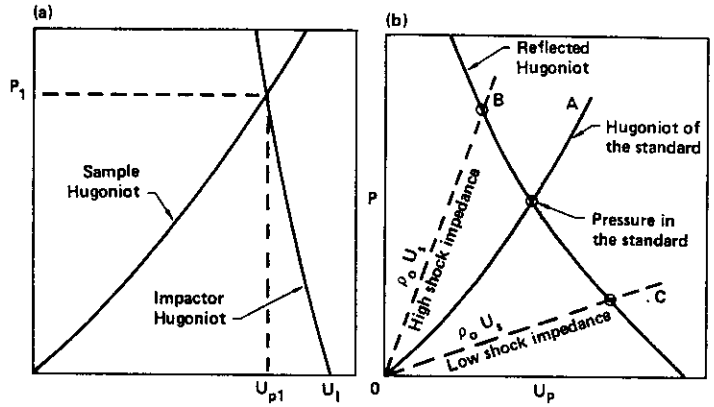

Ross -- Fig. 7

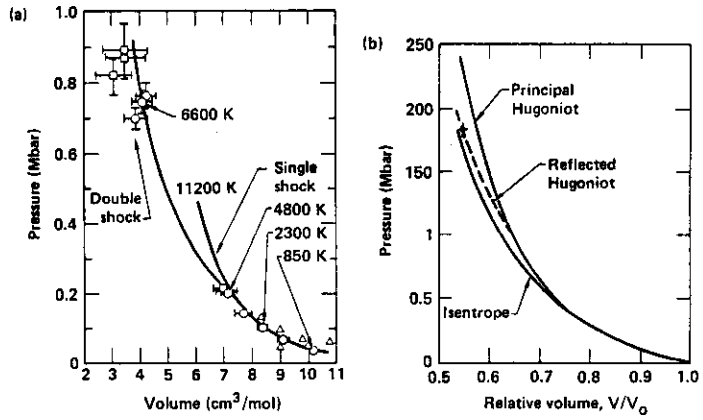

Ross -- Fig. 8

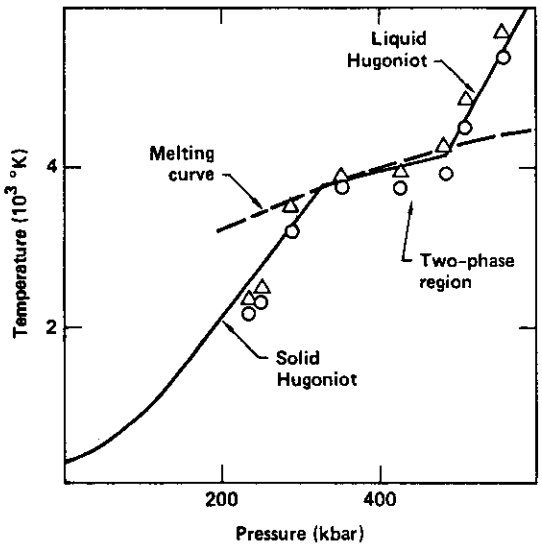

Ross -- Fig. 9

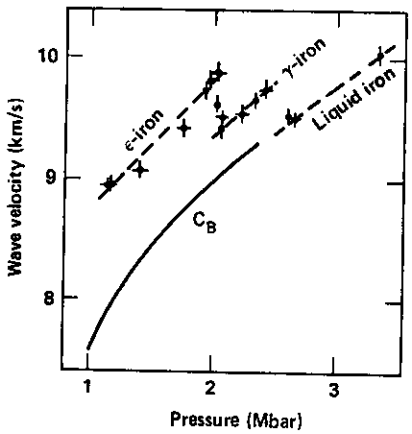

Ross -- Fig. 10

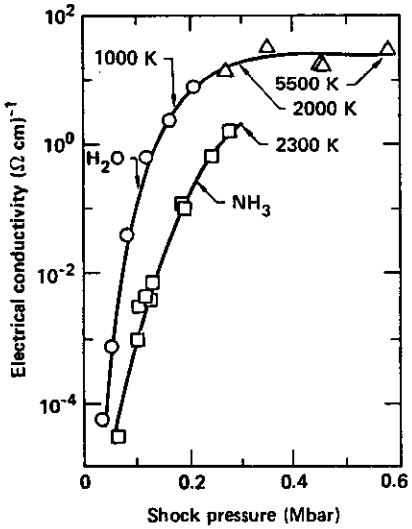

Ross -- Fig. 11

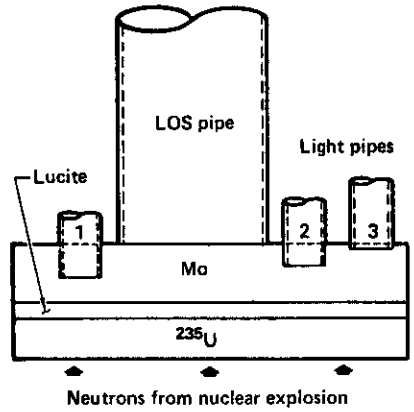

Ross -- Fig. 12

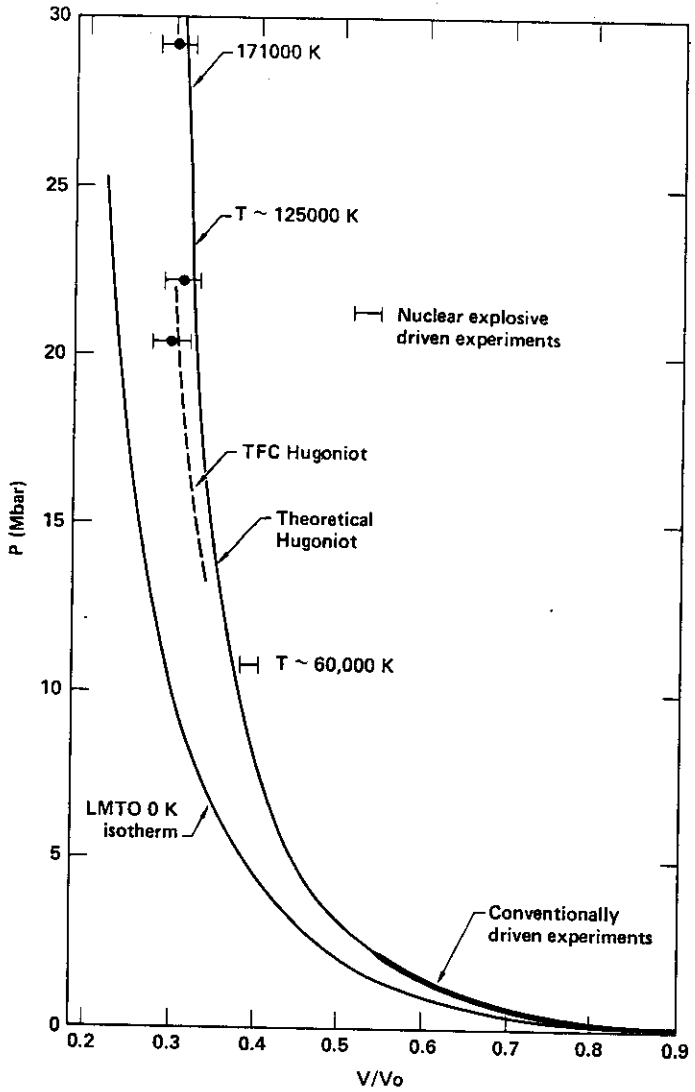

Ross -- Fig. 13

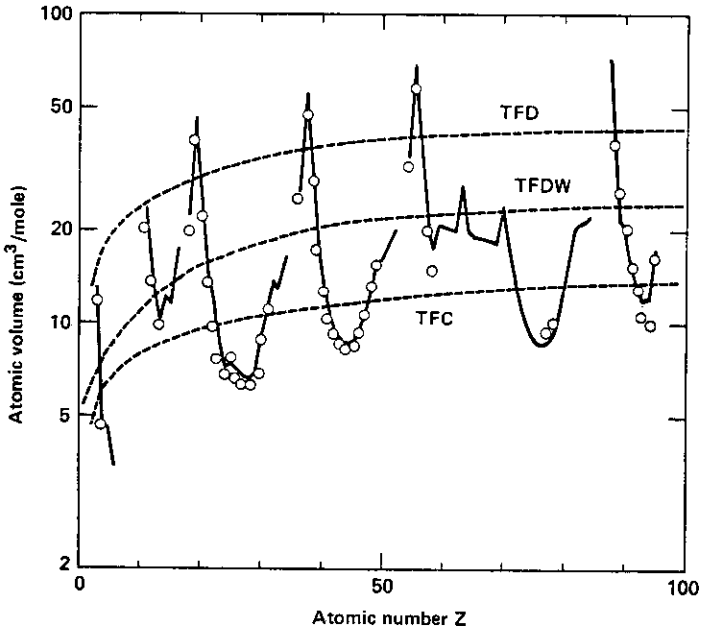

Ross -- Fig 14

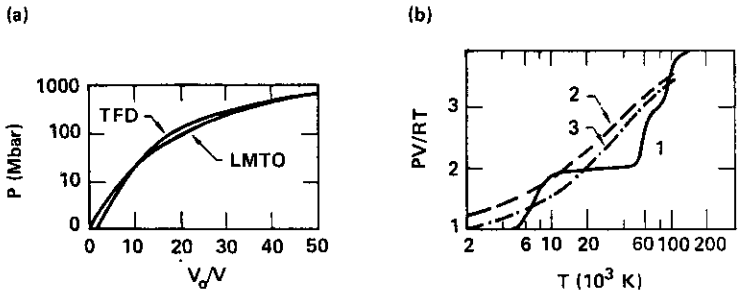

Ross -- Fig. 15

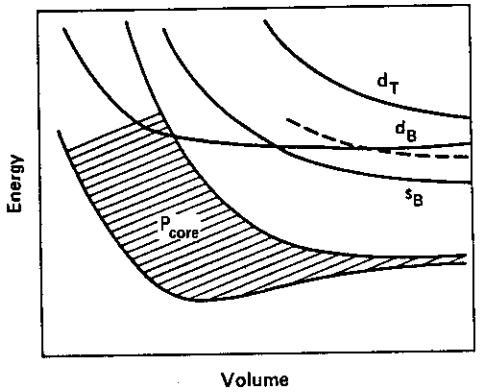

Ross -- Fig. 16

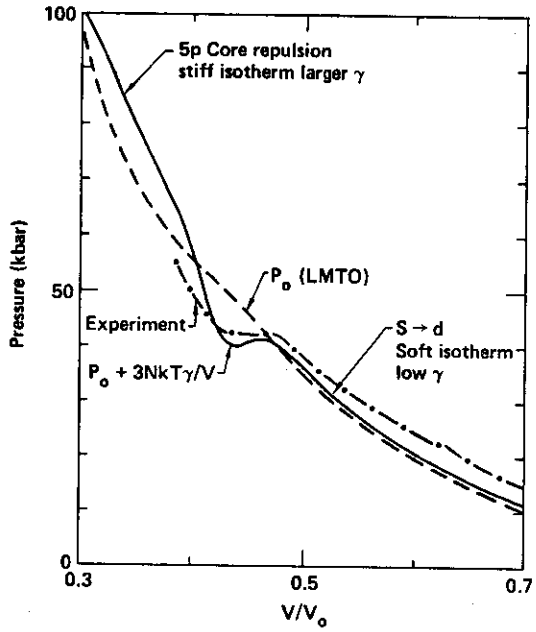

Ross -- Fig. 17

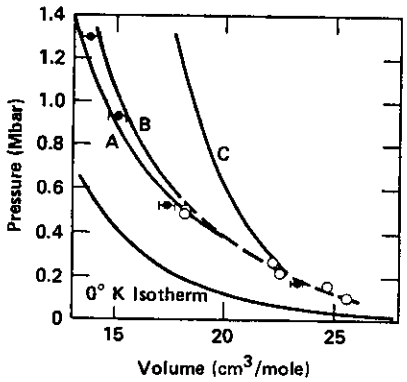

Ross -- Fig. 18

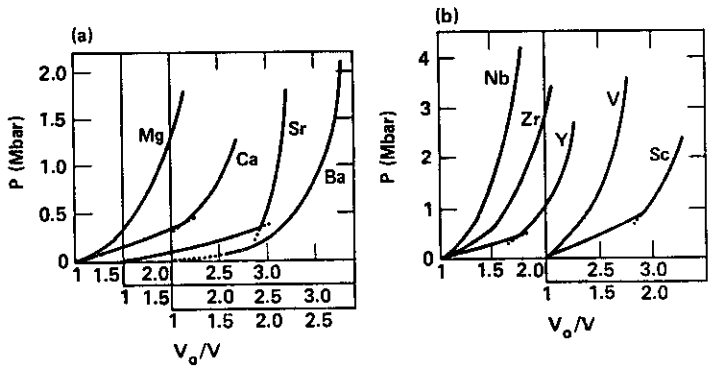

Ross -- Fig. 19

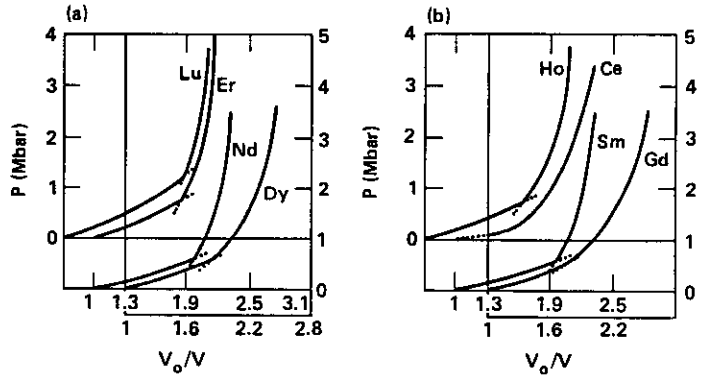

Ross -- Fig. 20

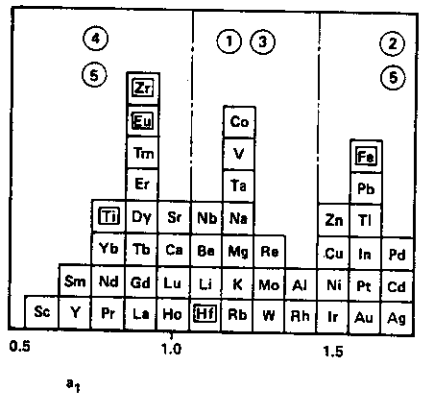

Ross -- Fig. 21

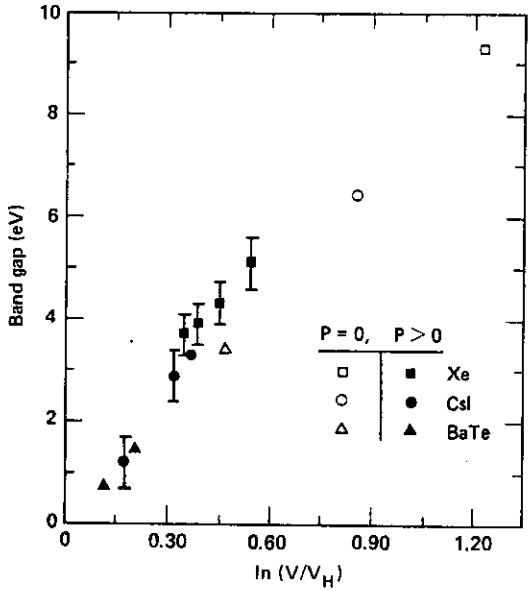

Ross -- Fig. 22

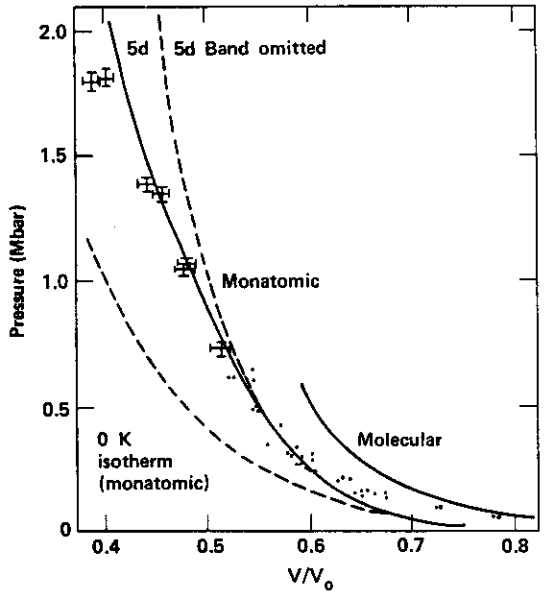

Ross -- Fig. 23

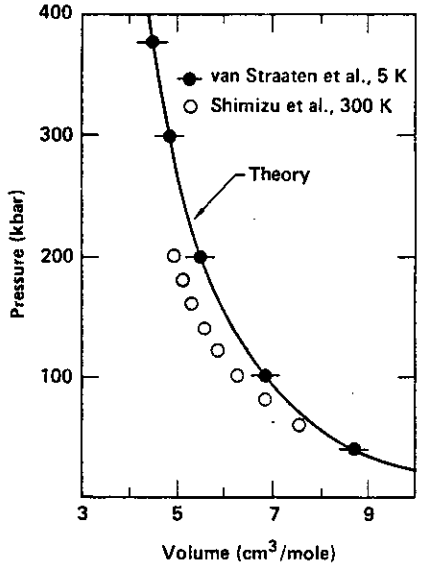

Ross -- Fig. 24

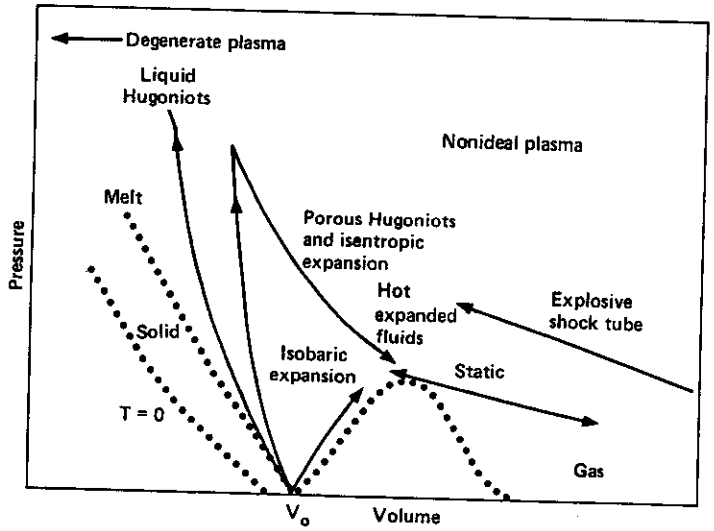

Ross -- Fig. 25

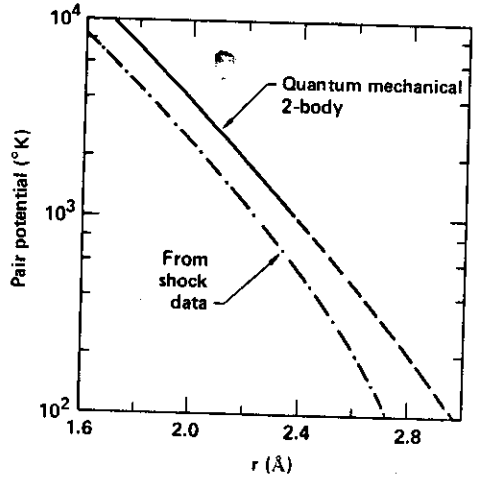

Ross -- Fig. 26

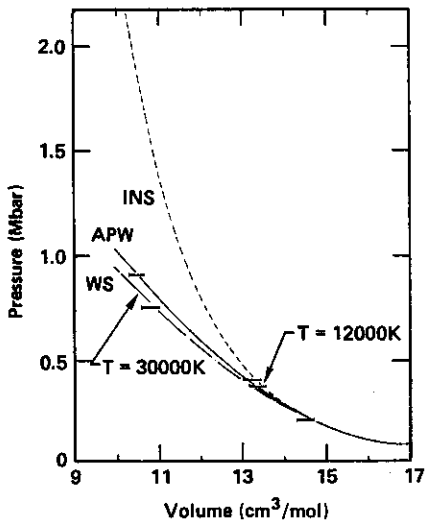

Ross -- Fig. 27

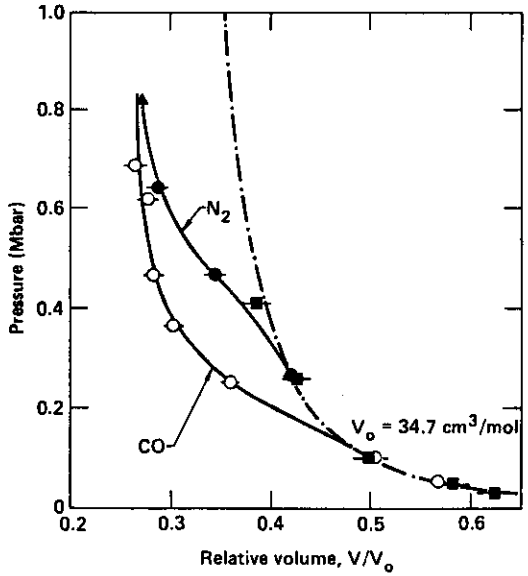

Ross -- Fig. 28

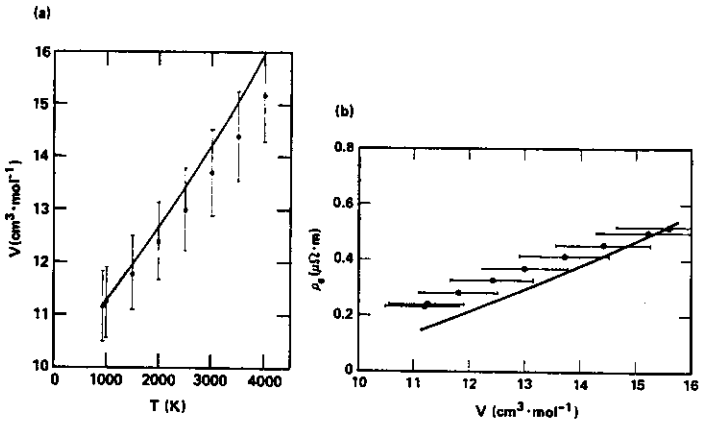

Ross -- Fig. 29

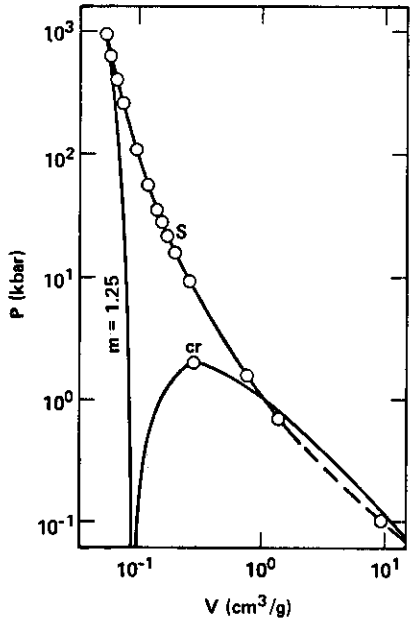

Ross -- Fig. 30

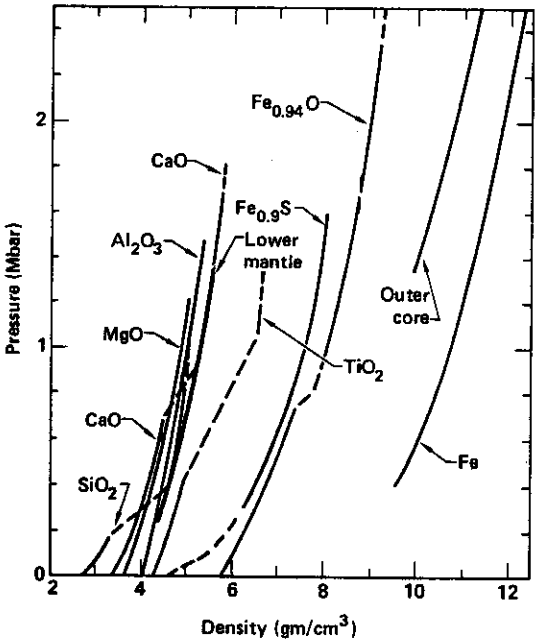

Ross -- Fig. 31

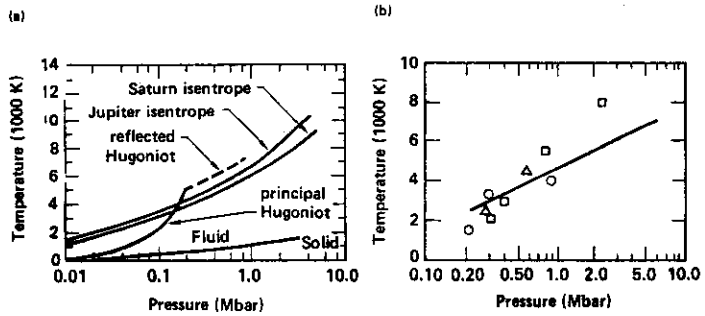

Ross -- Fig. 32